MXene-Based Anodes for Metal-Ion Batteries

Michael Greaves,[a] Suelen Barg,*[a] and Mark A. Bissett*[a]

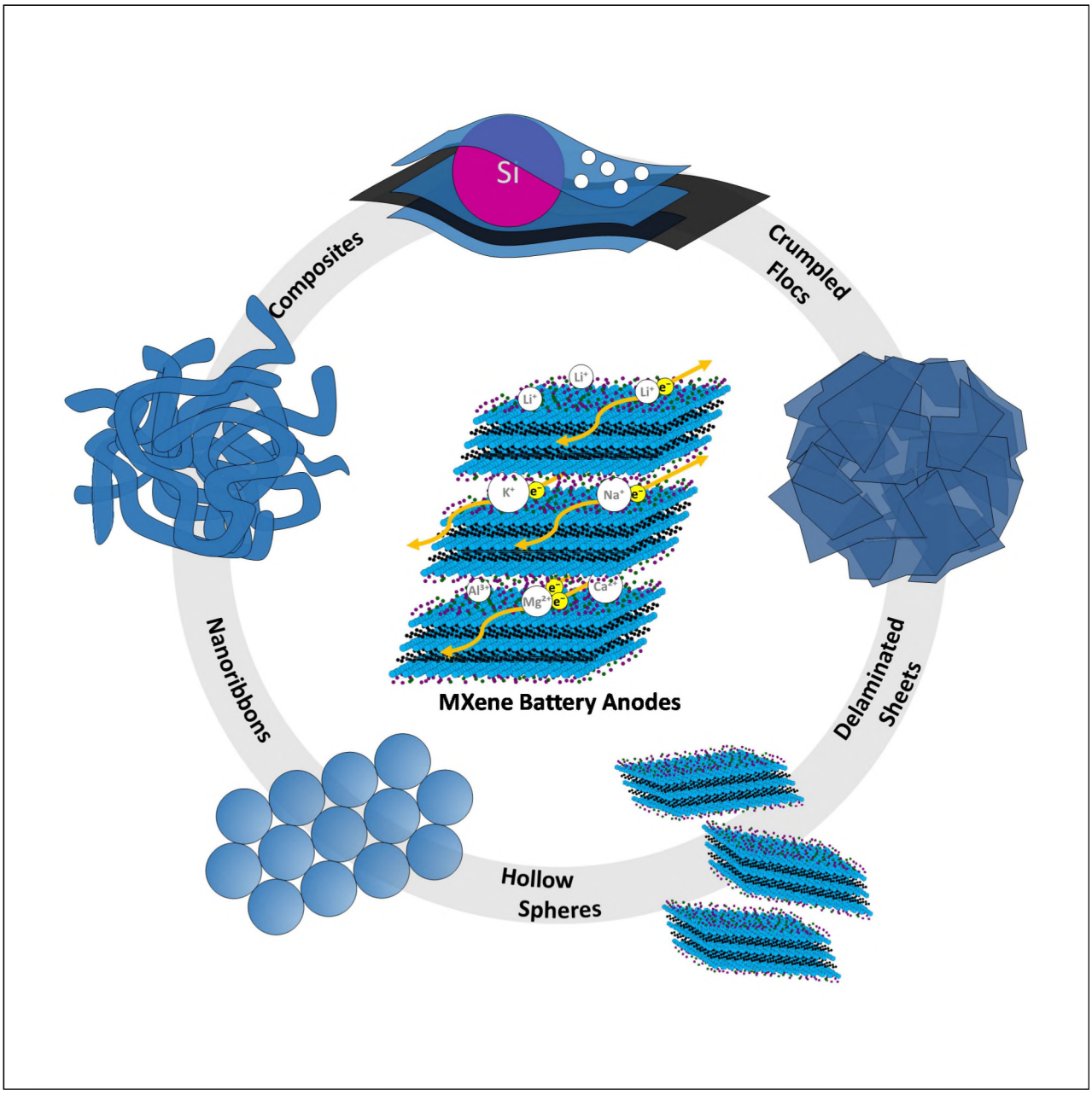

2D transition metal carbides and nitrides (MXenes) are electrochemically active materials capable of exhibiting pseudocapacitance. Multilayer MXenes are similar to graphite, but with larger interlayer spacing and surface functionalities which allow them to readily disperse in water and undergo a range of reactions without compromising their electrical conductivity. The large interlayer spacing enables MXenes to readily intercalate large ions, and form composites with materials such as graphene, metal oxides, transition metal dichalcogenides and silicon, with which they make electrodes able to deliver exceptional capacities at high power rates over thousands of cycles. Research into MXenes for energy storage has grown exponentially since 2011, and it is now necessary, especially for readers new to the field, to review progress made in more specific areas. This critical review will therefore analyse the progress made in developing MXene-based batteries, focusing solely on anodes developed for metal-ion batteries such as Li-ion, Na-ion and K-ion.

1. Introduction

Recent decades have seen great advancement in both the growth of the electronics market, and societal awareness of global pollution and climate change. These have been met with ambitious goals from both the public and private sector; low-carbon, high performance technologies must be developed and implemented within the coming decades in order for people to remain safe and companies to stay competitive.[1] At the heart of both the electronics and renewable energy markets is the issue of energy storage. Portable electronic devices are limited by the shape, size, capacity and power of their batteries, and the outputs of wind and solar power are limited by fluctuating weather conditions. Therefore, novel energy storage devices must be developed for both the next generation of portable electronics and large-scale grid storage.[2,3]

MXenes are two-dimensional (2D) transition metal carbides and nitrides with the general formula $M_{1+33}XT_X$ or $M_{n+1}X_nT_X$ ($1 \leq n \leq 3$), where *M* denotes an early transition metal (such as Ti, V, Mo, Sc, Nb, etc.), *X* denotes carbon and/or nitrogen, and T_X represents functional groups which inevitably arise on the surface during synthesis (usually O, OH and/or F). Conventional MXene synthesis involves the removal of *A* (typically Al) layers from MAX phase layered ceramics ($M_{n+1}AX_n$) using HF or HF precursors (usually LiF + HCl). Alternative, fluoride-free syntheses of MXenes is a growing field of research and a comprehensive review of recent synthesis progress and the properties of different MXenes was recently written by Barsoum *et al.*[4] As layered materials, multi-layered MXenes have been thoroughly investigated as a potential replacement for graphite in conventional Li-ion batteries, but like a number of other 2D nanomaterials MXenes exhibit pseudocapacitance, and so have also been investigated for use as electrodes for supercapacitors. The difference between these two energy storage systems has historically been that batteries store energy electrochemically, while supercapacitors store energy electrostatically. However, the field of energy storage research is moving exceptionally quickly, and because of this there has developed a degree of confusion within the scientific community about the criteria which determine whether a device is either a battery or a supercapacitor.[5,6] Most reviews of MXenes in energy storage have sidestepped this blurred distinction by reviewing both technologies,[7–12] but while these reviews are useful to those wishing to gain a broader perspective, they provide insufficient detail for readers who wish to understand the current state of research into either batteries or supercapacitors specifically. Therefore, the present review shall focus on works which self-identify as battery research, and discuss progress with the assumption that these MXene-based electrodes could take the place of graphite in a set-up not dissimilar from a conventional Li-ion battery (Figure 1). Whether this assumption holds true can be established at a later date, but here it serves as a simple way to recognise a distinction which has already arisen in the literature.

[a] *M. Greaves, Dr. S. Barg, Dr. M. A. Bissett*
Department of Materials, National Graphene Institute, University of Manchester, Oxford Road, Manchester, M13 9PL, United Kingdom
E-mail: suelen.barg@manchester.ac.uk
mark.bissett@manchester.ac.uk

2. Li-Ion Batteries

2.1. The Potential Usefulness of MXenes

First developed in 1991, lithium-ion (Li-ion) batteries charge and discharge *via* a "rocking chair" mechanism, in which Li^+ ions migrate back and forth between lithium-containing (e.g., $LiCoO_4$ or $LiFePO_4$) and carbon-based (usually graphite) electrodes. Over the past few decades, lithium-ion batteries have become so ubiquitous in rechargeable technologies that their development was deemed good enough to win the 2019 Chemistry Nobel Prize. The success of Li-ion batteries lies in their high energy density and cyclability, low self-discharge, and their effective use of cheap and abundant graphite anodes. However, graphite anodes do not allow fast enough solid-state diffusion to achieve the high power outputs necessary for some novel applications, and while the lithiation potential of graphite is very low, which is good for producing a high cell voltage (cell voltage = cathode voltage − anode voltage), it is low enough to enable the formation of lithium dendrites which are both flammable and impose a limitation on the cycling stability of cells.[13,14] As a potential alternative, MXenes have a slightly higher lithiation potential, and much wider interlayer spacing ($\approx$1 nm *vs.* $\approx$3 Å)[15,16] which can further be expanded through the use of different synthesis methods, pillaring, chemical modification, and/or complete delamination.[4,17,18]

This allows for the quick and facile intercalation of Li^+ and other metal ions (such as Na^+ and K^+, which shall be discussed later) with minimal lattice distortion, which improves both rate performance and cycling stability (Figure 1).[12]

The most significant difference between MXene and graphite anodes lies in their energy storage mechanisms. Unlike graphite, MXene-based anodes exhibit pseudocapacitive characteristics in their cyclic voltammetry (CV) and charge-discharge curves,[5,19] which benefits the rate performance of anodes but also necessitates some important considerations when examining results. Considering the illustration of typical galvanometric charge-discharge data in Figure 1b as a typical example, it should be noted that materials which are intended to act as battery anodes are in fact acting as cathodes in a half-cell (hence, they show a positive potential against Li/Li^+). Therefore, to assess their delithiation characteristics one must examine the charging curves (those with a positive gradient). It is important to bear this in mind when examining the literature because the delithiation (charging) half-cell curves of MXenes often have steeper slopes and higher potentials than the lithiation (discharge) curves, and may display a lower capacity due to poor coulombic efficiency (especially in the first cycle), which allows for exaggerated reports of good performance. It has become common in the literature to focus on the discharge behaviour of half-cells,[20] but this is especially inappropriate for pseudocapacitive materials which, unlike conventional battery anode materials, do not exhibit distinct voltage plateaus in their charge and discharge curves, and so in fact do not delithiate with the low voltages praised in some discussions. Another potential source of exaggerated performance is in the voltage window swept. In a Li-ion full cell, the anode should ideally not operate far outside of the range 0.5–1.5 V *vs.* Li/Li^+ in order to maximise the overall cell voltage without risking Li dendrite formation (which occurs as the electrode voltage approaches 0 V *vs.* Li/Li^+), but it is common practice in fundamental research studies to sweep far outside of this range to demonstrate that there are no further redox potentials. For conventional battery materials, with large plateaus in their charge-discharge curves, this does not have a significant effect on the reported capacity because the slope becomes very steep beyond the final redox plateau. However, when examining pseudocapacitive electrodes, the increased voltage can provide a significant contribution to the amount of charge stored. As discussed by Eftekhari,[20] this type of reporting is common in anode research, and is suitable for fundamental studies, but it is key for the community to remain aware of this, and to understand how it may affect the implementation of MXene anodes in commercial batteries.

2.2. MXenes as Electrode Active Material

Theoretical and experimental studies have found that the electrical and electrochemical characteristics of MXenes are highly dependent on their surface groups (T_X).[21–26] For instance, Tang, *et al.* found that even the configuration – much less the quantity – of OH and F terminations is able to determine whether $Ti_3C_2T_X$ is metallic or semi-conductive.[26] Many of these effects, while significant, are not seen experimentally due to the unavoidable mixing of O, OH and F terminations,[27] and the practical effects that altering the surface groups will often have on battery performance are with regard to facilitating high rate intercalation and adsorption, and the modulation of electrode voltage and/or capacity. While other MXenes show comparable theoretical performance,[28] Ti_3C_2 is by far the most studied and well understood. Bare Ti_3C_2 has proven to be the most ideal for energy storage with a number of ions, exhibiting higher theoretical capacities, lower intercalation potentials, and faster ion diffusion than its terminated derivatives. Nevertheless, bare MXenes oxidise very quickly, so realistically the best capacities are found in O- (which can adsorb multiple layers of Li),[25] followed by HO- and F-terminated MXenes[23,26] (with the

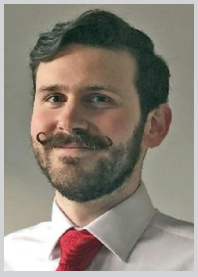

Michael Greaves obtained his MSci (Hons) in Chemistry from the University of Bristol, and is currently working towards a PhD in Nanoscience at the Graphene NOWNANO CDT, University of Manchester. His research focuses on novel electrode fabrication techniques using MXenes.

Dr. Suelen Barg obtained her PhD in Process Engineering, in the area of colloidal processing of advanced ceramics, at the University of Bremen. From 2010 to 2014 she was a postdoctoral associate and research fellow at Imperial College, where she studied new methods to assemble graphene-based materials into three-dimensional structures and composites. Since 2015, she has been a lecturer at the University of Manchester, where she leads a research group (Nano-3D) on the design and manufacturing of advanced nanostructured materials using colloidal processing (with focus on 3D printing) for their use in renewable energy, bio-medical and aerospace applications.

Dr. Mark A. Bissett obtained his PhD in Nanotechnology from Flinders University (Australia) in 2011. In 2012 he joined the Institute for Materials Chemistry and Engineering in Kyushu University (Japan) as a postdoctoral researcher and in 2014 he joined the University of Manchester in the Department of Chemistry, before moving to the Department of Materials. His research group focuses on the formulation and integration of low-dimensional materials, particularly graphene and other 2D materials, into electrochemical energy storage applications. This includes the synthesis, functionalisation and characterisation of these nanomaterials and their integration into devices such as photovoltaics, batteries, and supercapacitors.

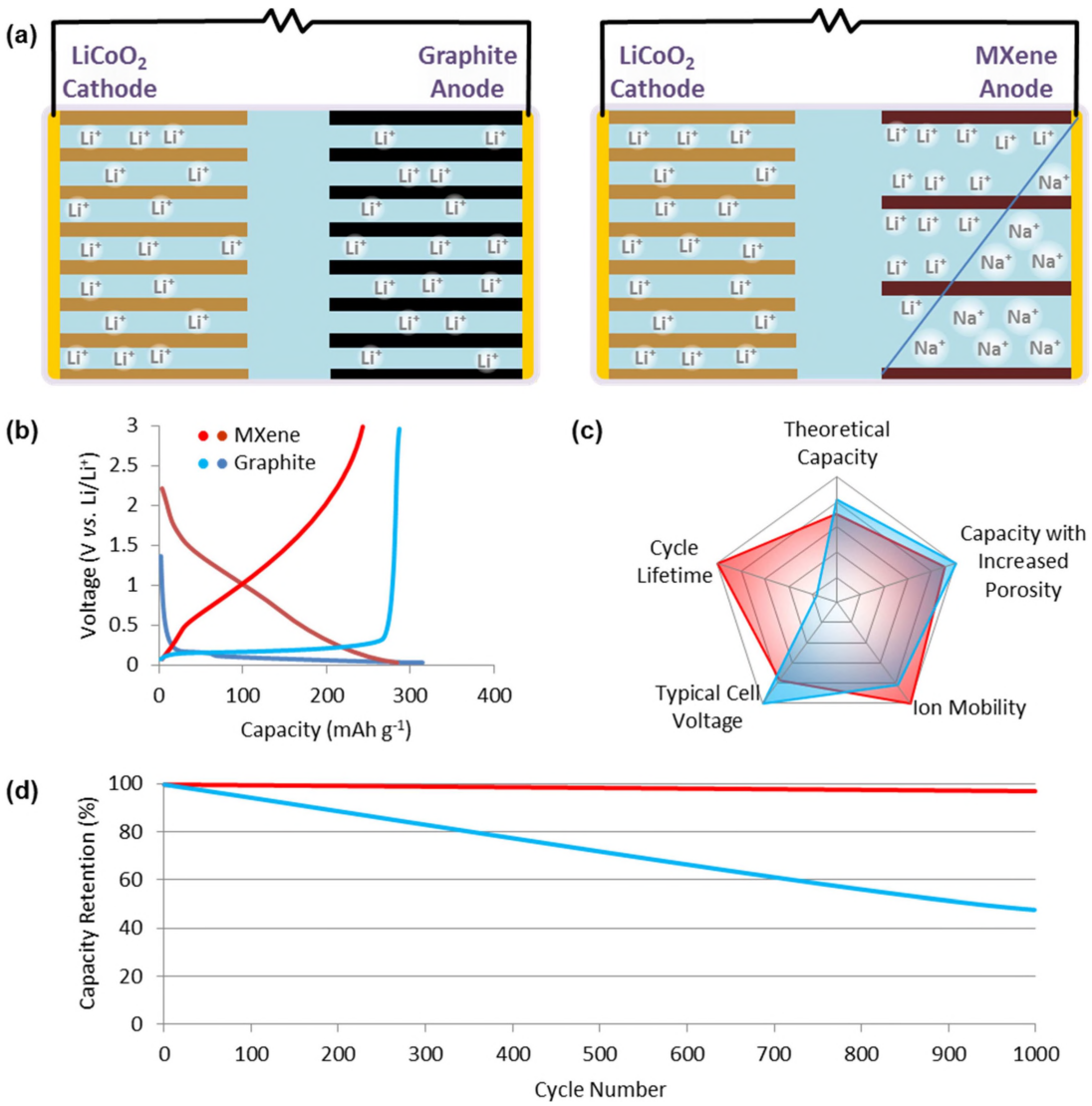

Figure 1. An illustration of the key differences between graphite and MXene electrodes. (a) Although the majority of research only reports on MXene-based anodes tested in half-cells, like graphite, these could be paired with a typical cathode (such as $LiCoO_2$) to make a full-cell. However, unlike graphite, MXenes are also suitable for use with Li alternatives, such as Na. (b) Half-cell charge-discharge curves suggest that MXene anodes will not provide as high a voltage as graphite in a full-cell, but could exhibit much better rate performance and cycling stability (c, d).

exception of special cases where normal functional groups have been substituted by another element or molecule such as Si).[29] This hierarchy of capacities is quite convenient for those who perform fluorine-free MXene syntheses,[30–34] as OH terminations can be removed by lithiation (which occurs during initial charge of a Li-ion battery) or annealing, and potentially be substituted by O terminations.

Table 1 summarises the electrochemical performance of a selection of bare MXenes in Li-ion cells. Although M_2C MXenes have the highest theoretical capacities,[23] they also tend to be less stable with regards to oxidation.[35] For this reason, $Ti_3C_2T_X$ continues to be significantly more common in the literature than its higher capacity counterpart, Ti_2CT_X. Initial computations attributed a theoretical capacity of 320 mAh g^{-1} to Ti_3C_2, assuming it would adsorb two Li adatoms per formula unit to make $Ti_3C_2Li_2$,[15] but later calculations showed it could adsorb a monolayer of up to 2.8 Li per formula unit, delivering a specific capacity of 447.8 mAh g^{-1}.[36] Experimental work from 2013 got close to this theoretical limit with a capacity of 410 mAh g^{-1}, which was attained by filtering a colloid of delaminated flakes to make a 'paper' electrode.[37] This work, by Mashtalir *et al.*, managed to increase the interlayer spacing of $Ti_3C_2T_X$, Ti_3CNT_X and $TiNbCT_X$ by intercalation of hydrazine monohydrate, urea and dimethyl sulfoxide (DMSO), and in the case of DMSO complete delamination of $Ti_3C_2T_X$ was achieved *via* sonication. Mashtalir *et al.* hypothesised that, as well as providing lower adsorption barriers,[38] delamination was able to provide a significant increase in capacity because it enabled the reversible formation of a unique solid-electrolyte interphase (SEI) during cycling. It is possible that a very recent work by Shen *et al.* has shed some light on this, as they achieved facile Li metal plating on porous, 3D-printed $Ti_3C_2T_X$ substrates.[39] With

Table 1. Summary of electrochemical performances of bare MXenes as electrode active material in Li-ion cells.

Material	Ref.	Capacity/ mAh g^{-1}	Rate	Notes
$Ti_3C_2T_X$	[40]	100	30 mA g^{-1}	Measured after 50 cycles
	[41]	203	0.2 A g^{-1}	Dropped and regained after 500 cycles
	[42]	134	1 C	106 mAh g^{-1} after 100 cycles
		90	3 C	83 mAh g^{-1} after 100 cycles
		48	10 C	68 mAh g^{-1} after 100 cycles
Ti_3C_2	[36]	447.8	–	Theoretical
Ti_2CT_X	[43]	225	C/25	
		110	1 C	Retained for 80 cycles at 1 C
Ti_3CNT_X	[44]	170	0.5 A g^{-1}	310 mAh g^{-1} after 1000 cycles
		140	1 A g^{-1}	200 mAh g^{-1} after 1000 cycles
		110	2 A g^{-1}	150 mAh g^{-1} after 1000 cycles
$Hf_3C_2T_X$	[45]	130	0.2 A g^{-1}	Retained after 200 cycles
Nb_2CT_X	[46]	170	1 C	Measured after 150 cycles
		110	10 C	
$Nb_4C_3T_X$	[47]	310	0.1 A g^{-1}	380 mAh g^{-1} after 100 cycles
		116	1 A g^{-1}	320 mAh g^{-1} after 100 cycles
V_2CT_X	[46]	260	1 C	Measured after 150 cycles
		125	10 C	

enough space, multiple layers of dendrite-free lithium were able to grow on $Ti_3C_2T_X$ (presumably facilitated by O terminations), and this could be what was able to occur between MXene sheets upon the delamination performed by Mashtalir *et al.* The significance of this recent work by Shen *et al.* should not be overlooked, as it serves not only to put forward a mechanism by which delamination can improve the capacity of MXenes, but also to show that $Ti_3C_2T_X$ can act as an effective substrate on which to grow Li metal anodes which do not form hazardous dendrites during cycling. With further development, this could lead to Li-ion batteries with maximal voltage and a capacity up to 3860 mAh g^{-1}.[39]

2.3. Chalcogenide/MXene Composites

2.3.1. Oxidised MXene

As highly conductive 2D materials, many MXenes are capable of acting as scaffolds for materials which exhibit desirable electrochemistry but suffer poor electrical conductivity and/or large volume changes upon reaction with Li^+. While carbon nanomaterials have been exploited for this purpose in a number of studies,[48–53] MXenes are hydrophilic – meaning they can be processed in aqueous solvents – and are able to participate in a wide range of chemistry without sacrificing conductivity, allowing for composite components to be more thoroughly mixed and to be linked by stronger connections *via in situ* synthesis. One simple way to achieve this is to oxidise a carbide MXene and thus produce nanoparticles of an electrochemically active metal oxide on the surface of conductive carbon sheets. This was first demonstrated by Naguib *et al.* in the oxidation of $Ti_3C_2T_x$ to form TiO_2/C,[54] and since then a number of MXenes have been partially oxidised so that the metal oxides can be formed without full conversion to amorphous carbon.[41,55–57] For example, Zhang *et al.* were able to combine the good rate performance and cycling stability of MXenes with the low delithiation potentials of TiO_2 and Nb_2O_5 in TiO_2@$Ti_3C_2T_x$, Nb_2O_5@Nb_2CT_x and Nb_2O_5@$Nb_4C_3T_x$ composites.[56,58] Partially oxidising MXenes demonstrates a facile approach to electrode fabrication, and recent developments in our understanding of MXene oxidation (often considered a drawback of MXenes in application)[35,59–63] readily prepare the scientific community to explore and optimise these routes further.

Building upon this method, $Ti_3C_2T_X$ has also been oxidised in the presence of alkali hydroxides to produce $Li_4Ti_5O_{12}$ and $Na_{0.23}TiO_2$ composites (Figure 2a, b).[64,65] Under ambient alkali conditions, $NaO_{23}TiO_2$ formed on the surface of Ti_3C_2 as nanobelts, which sat between MXene layers like filling in a sandwich (Figure 2a), preventing agglomeration and allowing a capacity comparable to the theoretical capacity of sodium titanate (178 mAh g^{-1}) to be retained after 4000 cycles at 5 A g^{-1}.[65] Other sodium titanates have previously exhibited pseudocapacitive energy storage mechanisms,[66] and so it should be no surprise that electrochemical tests of $NaO_{23}TiO_2$/Ti_3C_2 produced results similar to those of pristine $Ti_3C_2T_X$ (Figure 2c, e). However, the composite does show improved capacity and cycling stability compared to both its individual components; an improvement which could be attributed to the high ion accessibility and prevention of volume expansion that are afforded by the composite's unique morphology (discussed further in Section 4 of this review). Lithium titanate ($Li_4Ti_5O_{12}$, LTO) is a high power commercial anode material which suffers from reduced cell voltage (lithiation and delithiation potentials of 1.55 and 1.58 V *vs.* Li/Li$^+$) and capacity compared to graphite.[14] Under high temperature and pressure, Wang *et al.* produced a $Li_4Ti_5O_{12}$/$Ti_3C_2T_X$ composite which retained the electrochemistry of LTO (Figure 2d), and managed to achieve a capacity comparable to the theoretical capacity of pure LTO (178 mAh g^{-1}) at a high rate of 5 A g^{-1} after 500 cycles. The plateau contained in the charge-discharge curves (Figure 2f) also makes this electrode more suitable as a direct replacement for graphite, as it means that most of the capacity achieved within a 0–2.5 V window is retained when the electrode is swept through a smaller range. For example, the discharge capacity reported in the text written by Wang *et al.* is 331 mAh g^{-1} at 0.1 A g^{-1},[64] and this is corroborated by Figure 2f, But if only the range 0.3–1.7 V *vs.* Li/Li$^+$ is considered, then the delithiation capacity is still 190 mAh g^{-1}. While this may sound like a considerable decrease, similar examination of data from other pseudocapacitive electrodes often leads to much greater diminutions, and progress in reducing the active voltage window of MXene electrodes whilst retaining their good rate performance and cyclability could be very beneficial to the field.

Although it is inevitable that not all combinations of MXene/MXene oxide will be useful, with such a wide variety of possible MXenes available (*ca.* 30 synthesised so far),[4] these examples demonstrate a facile route to an expansive range of composites, with a selection of novel morphologies, that could

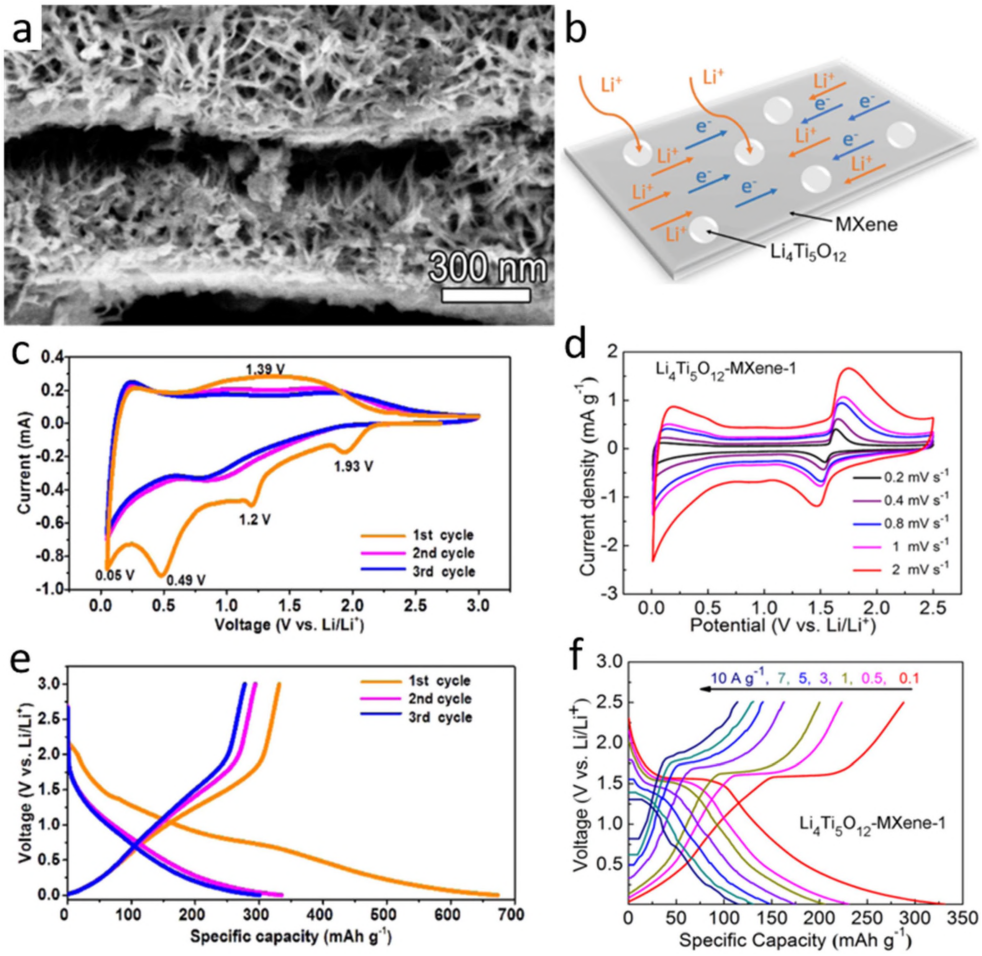

Figure 2. (a) SEM image of the "sandwich-like $NaO_{23}TiO_2/Ti_3C_2$" produced by Huang *et al.*[65] (b) Schematic illustration of the transfer of ions and electrons between layers of stacked $Li_4Ti_5O_{12}$–$Ti_3C_2T_X$ composite produced by Wang *et al.*[64] (c, d) Cyclic voltammograms of the $NaO_{23}TiO_2/Ti_3C_2$ (c) and $Li_4Ti_5O_{12}$-$Ti_3C_2T_X$ (d) composites. $NaO_{23}TiO_2/Ti_3C_2$ was scanned at 0.2 mV s^{-1}. (e, f) Charge and discharge curves of the two composites at different current rates. $NaO_{23}TiO_2/Ti_3C_2$ was scanned at 0.1 A g^{-1}. Copyright 2018 Elsevier.

potentially be very useful, not only for energy storage, but also for other applications such as catalysis and water desalination. However, as useful as it may be, the partial oxidation of MXenes is so facile that in many cases it is likely to be happening unintentionally and contributing to the electrochemical performances reported for pristine MXenes which have been exposed to oxidising agents, hydrothermal treatments or high temperatures. A good sign to look for this is the appearance of peaks in CV curves (e.g., at *ca.* 1.64 and 2.09 V *vs.* Li/Li^+ in oxidised $Ti_3C_2T_x$),[56] as small oxide crystals may not be detected by XRD, and the lasers used to produce Raman spectra have been known to stimulate oxidation, diminishing the reliability of Raman spectroscopy as a method for the detection of previously oxidised MXene. On the other hand, cyclic voltammetry should detect any metal oxide present in significant enough quantities to have an effect on electrochemical performance.

2.3.2. Other Chalcogenide Composites

Direct chemical binding of oxides can alternatively be sidestepped, and oxide hybridisation of MXenes can be achieved through alternated filtration or spray coating, as was demonstrated by Zhao *et al.* in $Ti_3C_2T_x/Co_3O_4$ and $Ti_3C_2T_x/NiCo_2O_4$ composites. Here, $Ti_3C_2T_X$ is effectively acting as a multifunctional binder to produce highly conductive, flexible electrodes without any extra additives. Although at relatively high voltage (plateau at *ca.* 2 V *vs.* Li/Li^+), $Ti_3C_2T_x/Co_3O_4$ electrodes made in 1:2 weight ratio exhibited twice the low-rate capacity of $Ti_3C_2T_X$ or Co_3O_4 alone, and significantly improved rate performance up to 3 C, demonstrating the ability of these metal oxides to act synergistically even without thorough mixing or chemical binding.[67]

Among transition metal oxides considered for Li-ion battery anodes, iron(II,III) oxide (Fe_3O_4) has one of the highest theoretical specific capacities (926 mAh g^{-1}), lowest cost, and is environmentally safe. Wang *et al.* intercalated Fe_3O_4 nanoparticles into multilayer $Ti_3C_2T_x$ using 6 hours of ultrasonication, achieving reversible capacities up to 747 mAh g^{-1}

(2038 mAh cm^{-3}) after 1000 cycles at 1 C – much greater than those of either Fe_3O_4 or $Ti_3C_2T_X$ alone. The value added by compositing these materials was highly dependent on their ratio, with the best performance coming when Fe_3O_4 and $Ti_3C_2T_X$ were combined in a 2:5 weight ratio.[68] In this and a similar work,[69] a weight ratio of 1:1 was only able to help cycling stability and did not significantly improve capacity or rate performance. Another way to achieve a similar microstructure is by delamination of the MXene and subsequent filtration of a mixed MXene-metal oxide colloid, as demonstrated by Lu *et al.* Not only were similar improvements seen in their MXene/$CoFe_2O_4$ composite electrode, but the filtration technique allowed them the control to not include $CoFe_2O_4$ in the bottom portion of the electrode, so that pure MXene could act as a current collector with high electrical and ionic conductivity.[70]

Sn^{4+} is also an attractive ion to use in Li-ion batteries because of its potential capacity, cost, and environmental benignity. However, like many transition metal oxides (TMOs) it has poor conductivity, ionic diffusivity, and rate performance. Three particular MXene composites, which have been made using an amorphous Sn(IV) nanocomplex,[71] hydrothermally added SnO_2,[72] and atomic layer deposition of SnO_2[73] achieve moderate reversible capacities, but at low rates; 544 mAh g^{-1} at 0.5 A g^{-1},[71] and 360 mAh g^{-1} at 0.1 A g^{-1}.[72] They also show similarly poor rate performance with little evidence of long cycle lifetime. Although, when the $SnO_2/T_3C_2T_x$ composite made by atomic layer deposition was further coated with HfO_2, it exhibited a much more impressive capacity of 843 mAh g^{-1} at 500 mA g^{-1}.[73] A proposed explanation for the poor performance of $Sn^{4+}/Ti_3C_2T_X$ composites is the superficial distribution of Sn^{4+}. Self-assembly of TMO/MXene composites has proved viable, as TiO_2 nanorods or SnO_2 nanowires are able to form micelle-like structures, stabilising suspensions of $Ti_3C_2T_x$ in THF. This scalable technique enables thorough intercalation of materials with different nanoscale morphologies, opening up ion pathways and preventing nanoparticle agglomeration. While the CV plots of Li-ion half-cells show sharp lithiation-delithiation peaks, the reversible capacities and rate performance of these electrodes were no better than those of other SnO_2 composites.[74]

Delaminated transition metal dichalcogenides are a family of 2D nanomaterials which have high lithium-ion storage capacities, but are often semi-conductive and swell upon ion intercalation, leading to poor rate and cycling performance. To combat these issues, 2D MoS_2 has been combined with titanium carbide MXenes *via* a number of different methods with some promising results.[75–78] For example, Chen *et al.* synthesised a MoS_2/MXene heterostructure by sulfurization of the MXene $Mo_2TiC_2T_x$ (in which the Ti atoms occupy the central plane of the crystal lattice) to make $MoS_2/Mo_2TiC_2T_X$.[76] The presence of MXene enabled MoS_2 to become metallic, and retention of the layered structure allowed strong Li–S interactions to facilitate fast intercalation. Lithium polysulfides – which can reduce cell lifetime through the *shuttle effect* – were effectively anchored by Ti and Mo, enabling 92% of a high initial capacity (548 mAh g^{-1} at 50 mA g^{-1}) to be retained after 100 cycles, which is 9.7× higher than pure MoS_2 electrodes.

Zheng *et al.*[75] synthesised MoS_2 nanosheets on the surface of multi-layered $Ti_3C_2T_X$ *via* a hydrothermal method (which also partially oxidised the MXene). At 20 wt% MoS_2, this composite exhibited good rate performance up to 3 A g^{-1}, but poor cycling stability. A common impediment to long cycling lifetime in all the electrodes reviewed in this work is MXene oxidation. Therefore, Wu *et al.* attempted to protect the surface of delaminated $Ti_3C_2T_x$ with carbon nanoplating in a hierarchical MoS_2/Ti_3C_2@C nanohybrid synthesised by a similar hydrothermal method (Figure 3a).[77] During MoS_2 synthesis, glucose was simultaneously reduced to carbon on the surface of $Ti_3C_2T_x$, removing the T-groups (F, O and OH) by substitution. The authors found that Ti_3C_2 is two orders of magnitude more conductive than reduced graphene oxide (rGO), and therefore it is able to significantly reduce the charge transfer impedance and greatly enhance the rate performance of MoS_2 (Figure 3b–d). After a large initial drop (which was in part attributed to the formation of Li_2CO_3 and alkyl carbonates, electrolyte decomposition, the trapping of Li atoms in MoS_2, and the formation of metallic Mo), very high capacities were reported over many cycles and at a range of current rates (Figure 3c–d and Table 2). Although the charge-discharge curves display no obvious voltage plateau, examination of Figure 3b indicates that the delithiation capacity between 0.3–1.7 V *vs.* Li^+/Li is approximately 570 mAh g^{-1}, which is still significantly higher than graphite thanks to the very high capacities exhibited in the wide voltage window of 0.01–3.0 V. The long-term cycling data also shows a capacity increase for the first few hundred cycles (Figure 3d), which despite a lack of experimental investigation is attributed by the authors to reversible electrolyte polymerisation and unknown changes in the electrode which enable ions to access an increasing number of adsorption sites. One of the most important insights gained from this work is the ability to protect Ti_3C_2 from oxidation using carbon nanoplating. Although the effectiveness of this protection is only characterised by the long-term cycling stability of the material, further research into the long-term stability of this composite under ambient conditions could be beneficial to all areas of MXene-related research, as their short shelf life remains a significant hurdle to MXenes being used in any commercial application.

In summary, a number of MXene/chalcogenide composites (summarised in Table 2) have been synthesised and tested for their use in Li-ion batteries, and they have all exhibited some improvement in gravimetric capacity. Approximately 2/3rds of those reviewed here have recorded maximum capacities greater than that of typical graphite anodes,[79] some even surpassing 1000 mAh g^{-1}.[67,77] Most of the composites reviewed here showed reasonable rate behaviour, but those which showed the best rate behaviour and cycle lifetime also exhibited quite strongly pseudocapacitive CV and charge-discharge profiles, meaning that large portions of their capacities are delivered at voltages too high for conventional Li-ion battery anodes.[65,67,77,80] Of particular note here is the MoS_2/Ti_3C_2@C composite presented by Xianhong Wu *et al.*, which was stable against oxidation due to its protective carbon layer, and

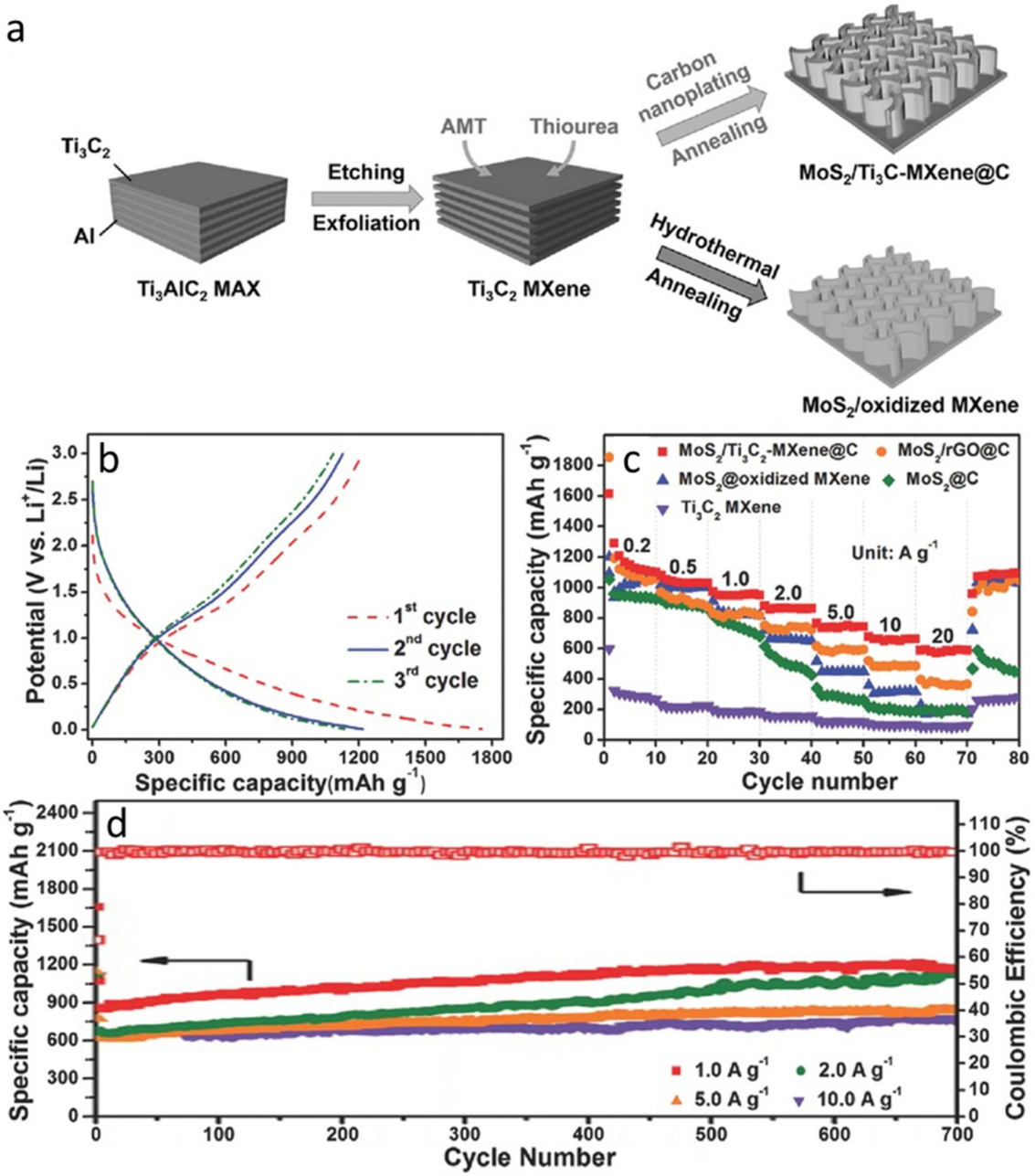

Figure 3. (a) The formation process of MoS_2/Ti_3C_2@C nanohybrids, which is achieved by assembling carbon coated few-layered MoS2 nanoplates on carbon-stabilized Ti_3C_2 MXene under hydrothermal conditions followed by annealing in Ar flow. Without carbon nanoplating, the Ti_3C_2 MXene is rapidly transformed to TiO_2 during the reactions. (b) Discharge-charge voltage profiles of MoS_2/Ti_3C_2@C electrodes for the first three cycles at a current density of 0.2 A g^{-1}. (c) Rate capability of MoS_2/Ti_3C_2@C, MoS_2/oxidised $Ti_3C_2T_X$, MoS_2/rGO@C, MoS_2@C and $Ti_3C_2T_X$ electrodes at current densities of 0.2–20.0 A g^{-1}. (e) Long-term cycling stability and Coulombic efficiency of MoS_2/Ti_3C_2@C electrodes at high current densities of 1.0, 2.0, 5.0 and 10.0 A g^{-1}. All tests conducted between 0.01–3.0 V.[77] Copyright 2017 Wiley-VCH.

exhibited phenomenal performance in all ways except for the wide voltage window over which its capacity was delivered.[77] It is clear that the high rate capability of MXenes is intrinsically linked to their capacitive behaviour,[81] and so future work should seek to optimise composites with materials that exhibit sharp redox peaks, where MXenes contribute by providing conductive networks and mechanical scaffolds.

2.4. Carbon and Silicon MXene Composites

As with other novel electrode materials, most MXene-based electrodes are fabricated from a mixture of active material, conductive carbon additives and a binder (usually in the form of 80% active material, 10% carbon black, and 10% polyvinylidene fluoride (PVDF) binder) to improve rate performance and mechanical strength. So in this sense most MXene-based electrodes are carbon composites, but a number of works

Table 2. Summary of electrochemical performances of chalcogenide/MXene composites in Li-ion cells.

Material	Ref.	Capacity/ mAh g^{-1}	Rate	Notes
Nb_2O_5@$Nb_4C_3T_X$	[56]	208	50 mA g^{-1}	94% retained after 400 cycles
TiO_2/$Ti_3C_2T_X$	[41]	267	0.2 A g^{-1}	Dropped and regained after 2000 cycles
TiO_2/$Ti_3C_2T_X$	[56]	124	50 mA g^{-1}	Retained after 400 cycles
TiO_2/Ti_2CT_X	[55]	389	0.1 A g^{-1}	Retained for 70 cycles
		337	0.5 A g^{-1}	Retained for 100 cycles
		297	1 A g^{-1}	Retained for 100 cycles
$NaO_{23}TiO_2$/$Ti_3C_2T_X$	[65]	178	5 A g^{-1}	Measured after 4000 cycles
$Li_4Ti_5O_{12}$–$Ti_3C_2T_X$	[64]	178	5 A g^{-1}	Measured after 500 cycles
$Ti_3C_2T_x$/Co_3O_4	[67]	50	20 C	Retained after 100 cycles
		1200	0.1 C	
$Ti_3C_2T_X$/$NiCo_2O_4$	[67]	1330	0.1 C	Retained after 100 cycles
		650	5 C	
		350	10 C	
Fe_3O_4@$Ti_3C_2T_X$	[68]	278	5 C	Measured after 800 cycles
		747	1 C	Measured after 1000 cycles
PVP–Sn(IV) @$Ti_3C_2T_X$	[71]	544	0.5 A g^{-1}	Measured after 200 cycles
SnO_2/Ti_3C_2/HfO_2	[73]	843	500 mA g^{-1}	Stable for $\geq$ 50 cycles
SnO_2/$Ti_3C_2T_X$	[72]	400	0.1 A g^{-1}	360 mAh g^{-1} after 200 cycles
Ag/Ti_3C_2 $(OH)_{0.8}F_{1.2}$	[80]	310	1 C	Measured after 5000 cycles
		150	50 C	
MoS_2/$Ti_3C_2T_X$	[75]	656	50 mA g^{-1}	70% retained after 50 cycles
		153	3 A g^{-1}	
MoS_2/$Mo_2TiC_2T_X$	[76]	90	5 A g^{-1}	92% retained after 100 cycles
		548	50 mA g^{-1}	
MoS_2/Ti_3C_2@C	[77]	580	20 A g^{-1}	95% retained after 3000 cycles at 20 A g^{-1}
		1130	0.2 A g^{-1}	

Table 3. Summary of electrochemical performances of carbon and silicon MXene composites in Li-ion cells.

Material	Ref.	Capacity/ mAh g^{-1}	Rate	Notes
Ti_2CO_2/ Graphene	[82]	426	–	Theoretical
rGO/$Ti_3C_2T_X$ film	[84]	221	50 mA g^{-1}	Stable for 275 cycles
		111	1 A g^{-1}	
rGO/$Ti_3C_2T_X$ foam	[85]	179	1 A g^{-1}	213 mAh g^{-1} after 1000 cycles
CNTs@Ti_3C_2	[89]	430	1 A g^{-1}	Measured after 300 cycles
		175	10 A g^{-1}	
$Ti_3C_2T_X$/ CNT	[92]	500	0.5 C	Measured after 100 cycles
	[90]	228	0.5 C	245 mAh g^{-1} after 100 cycles at 0.5 C
		132	5 C	75 mAh g^{-1} after 100 cycles at 5 C
Nb_2CT_X/ CNT	[90]	420	0.5 C	460 mAh g^{-1} after 100 cycles at 0.5 C
		320	2.5 C	430 mAh g^{-1} after 300 cycles at 2.5 C
		225	10 C	200 mAh g^{-1} after 100 cycles at 10 C
Mo_2C/CNT	[109]	560	0.4 A g^{-1}	Measured after 70 cycles
		75	10 A g^{-1}	Stable for 1000 cycles
Ti_3C_2/CNF	[93]	320	1 C	Retained after 2900 cycles at 100 C
		97	100 C	
Si@$Ti_3C_2T_X$	[102]	188	0.2 A g^{-1}	Measured after 150 cycles
Ti_3C_2/Si@-SiO_X@C	[107]	1444	0.5 C	76% capacity retained after 1000 cycles at 10 C
		510	10 C	
nSi/$Ti_3C_2T_X$	[106]	2100	1.5 A g^{-1}	1280 mAh g^{-1} after 275 cycles
nSi/Ti_3CNT_X	[106]	1600	1.5 A g^{-1}	1100 mAh g^{-1} (69% capacity) after 70 cycles
Si/$Ti_3C_2T_X$	[105]	2118	0.2 A g^{-1}	Measured after 100 cycles
		1672	1.0 A g^{-1}	Measured after 200 cycles
		890	5.0 A g^{-1}	Measured after 20 cycles
3:2 Si@C: $Ti_3C_2T_X$	[103]	1700	0.42 A g^{-1}	61% capacity retained after 150 cycles at 0.42 A g^{-1}
		941	4.2 A g^{-1}	
1:1 $Ti_3C_2T_X$:Si	[104]	450	1 C	Increased to 558 mAh g^{-1} after 500 cycles

(summarised in Table 3) have incorporated graphene or carbon nanotubes (CNTs) in a controlled manner to enhance the electrode performance and lifetime to an even greater extent.

Computational studies of MXene/graphene heterostructures (where graphene and MXene layers stack alternately) have found that graphene is able to prevent restacking in scandium, titanium and vanadium M_2CT_X MXenes, and enhance mechanical stiffness, Li adsorption strength, and electric conductivity without compromising on Li diffusive mobility. Ti_2CO_2/graphene and V_2CO_2/graphene heterostructures exhibit the strongest Li binding energies (−1.43 eV at 1.49 V and −1.78 eV at 1.93 V respectively), and are predicted to swell no more than 5% upon lithiation.[82,83] Experimental studies have seen the development of an rGO/$Ti_3C_2T_X$ electrode made by filtration of a mixed colloid,[84] and a range of 3D, porous rGO/$Ti_3C_2T_X$ foams made using hydrazine GO reduction.[85] Most of these composites are comparable to pure $Ti_3C_2T_X$ in their cycling stability and the variation in capacity with rate, but they consistently show significantly higher absolute values of capacity. Further discussion of these can be found in Section 4 of this review.

Carbon nanotubes (CNTs) are well researched as a material for use in composite electrodes because of their electrical conductivity, flexibility, and compatibility with 2D materials.[86,87] When combined with MXenes, they are thought to increase capacity, cyclability and power density by increasing electrical conductivity and improving the accessibility of ions *via* three main mechanisms:[88] (1) Bridging individual flakes to improve the conductive network through which both ions and electrons can travel;[89] (2) preventing the restacking of delaminated sheets; and (3) increasing the interlayer spacing of multilayer flakes (so called "pillaring").[90] Adding to their potential as a useful additive, CNTs are very easy to combine with MXenes, for example, by filtration of a mixed suspension, or by

alternated spray coating to make a sandwich-like assembly.[88,91] With an optimal $Ti_3C_2T_X$:CNT mass ratio of 1:1, such composites have been shown by Liu, *et al.* to be freestanding, flexible, and able to maintain a discharge capacity of 428 mAh g^{-1} at 0.5 C after 300 cycles in Li-ion half-cells; an improvement of more than 340% compared to CNTs or multilayer $Ti_3C_2T_X$ alone.[91]

When Ren *et al.* developed a synthetic route towards porous (or "holey") MXenes,[92] they found that the resulting increase in ion accessibility had little effect on the capacity when compared to pristine MXenes. However, by combining these MXenes with CNTs in flexible films they were able to produce electrodes whose capacity increased with cycling until a plateau of 1250 mAh g^{-1} was reached after *ca.* 250 cycles at 0.1 C. The capacity of a number of MXene/CNT composites increases over extended cycling (Figure 4d),[91,92] as seen in the MoS_2/Ti_3C_2@C composite above.[77] For example, the capacity of a composite produced by Mashtalir *et al.*[90] increased from 320 to 430 mAh g^{-1} over 300 cycles (beyond which further cycles were not measured). Assuming this phenomenon can be attributed to similar processes to those described by Wu *et al.*,[77] then similar cycling behaviour to the MoS_2/Ti_3C_2@C composite should be observed beyond the 300th cycle, in which a peak in capacity is seen at the point where the rate of increasing ion accessibility is overtaken by the rate of electrode degradation. However, this is not necessarily the cause of increasing capacity, and further study is needed. For instance, it could be attributed to thermodynamic effects caused by heating of the battery as it is cycled, in which case the capacity would drop again after a suitable period of inactivity.

Ex situ growth of CNTs followed by mixing often results in inhomogeneous products which exhibit highly capacitive electrochemical signatures. Therefore, in the same vein as similar work on carbon nanofiber (CNF) composites,[93] Zheng *et al.* have grown ferrocene-derived CNTs from the MXene surface *in situ* to form structures morphologically similar to a frieze carpet (Figure 4a and b). The capacity of these electrodes increased with cycling, plateauing at *ca.* 300 cycles (Figure 4d), and the removal of some F terminations, along with the redox potentials of iron, enabled a delithiation capacity of 164 mAh g^{-1} between 0.3 and 1.7 V *vs.* Li/Li^+ to be observed after 100 cycles at 1 A g^{-1} (3 C) (Figure 4c).[89]

The capacities of MXenes and carbons are typically on the order of 100 mAh g^{-1}, which has proven adequate for most commercial applications in the last few decades, but pales in comparison to other group 4 elements whose capacities exceed 1000 mAh g^{-1} but are withheld from commercialisation because of their very poor cycling and/or rate performance.[29,94,95] Therefore, as the next generation of energy storage devices are developed, it seems clear that MXenes and carbons will best serve as porous, conductive hosts to facilitate fast ion and electron transport about particles of another material which are free to expand/contract within the conductive framework. And given that MXenes are inherently more expensive to produce than most carbon allotropes, MXenes will most effectively be utilised in composites where their chemistry and interlayer spacing provide enhancements which conventional carbon scaffolds cannot.

Silicon is a well-studied anode material with an extremely high theoretical lithiation capacity of 4198 mAh g^{-1},[96] delithiation potential of *ca.* 0.4 V,[14] and practically unlimited natural abundance.[97] The main obstacles to application are its poor electrical conductivity,[98] lithiation/delithiation volume changes of $>300\%$,[99] low Li^+ diffusivity (ca. 10^{-14}–10^{-13} $cm^2 s^{-1}$),[100] and a continually growing SEI which both degrades the electrode

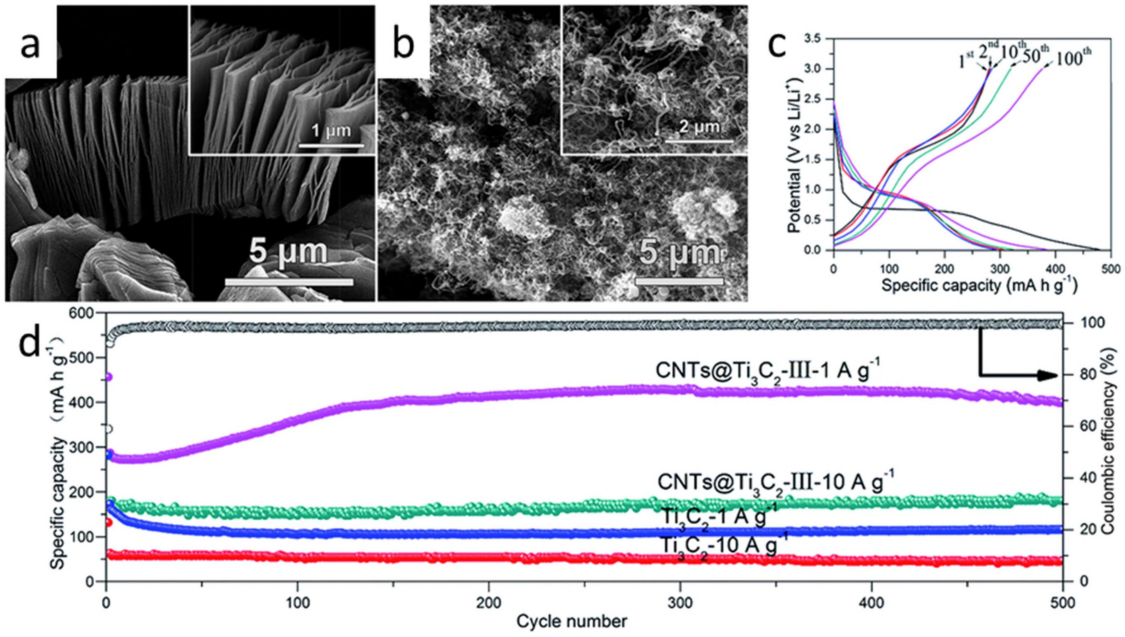

Figure 4. SEM micrographs of (a) $Ti_3C_2T_X$; and (b) CNTs grown on $Ti_3C_2T_X$ *via* 3 microwave irradiation cycles (CNTs@Ti_3C_2-III). (c) Galvanostatic charge-discharge curves of CNTs@Ti_3C_2-III at 1 A g^{-1}. (d) Reversible capacity of $Ti_3C_2T_X$ and CNTs@Ti_3C_2-III electrodes at 1 and 10 A g^{-1} in the range 0.01–3 V *vs.* Li/Li^+. Coulombic efficiency is plotted for the CNTs@Ti_3C_2-III electrode with 1 A g^{-1} only.[89] Copyright 2018 Royal Society of Chemistry.

and consumes electrolyte over a short number of cycles.[101] The use of MXenes to overcome these issues has seen a surge of interest in the last year (Table 3),[102–107] with titanium carbides being able to act as a multifunctional binder and reinforcement to silicon carbides,[103,108] and viscous MXene inks being able to provide high Si mass loading to thick film electrodes.[106] The first experimental example of a Si-MXene electrode was published by Kong *et al.* in December 2018.[102] Si-MXene composite electrodes fabricated by filtering a mixed colloid of $Ti_3C_2T_X$ and commercial Si nanoparticles (typically 20–60 nm in diameter), such as those produced by Kong, are easy to prepare and show considerable improvement upon Si or $Ti_3C_2T_X$ alone.[102,104,105] For example, Li *et al* produced a 1:1 $Ti_3C_2T_X$:Si composite electrode whose capacity inexplicably increased beyond the 200th cycle as it developed a progressively more capacitive character, and they were able to show that the MXene disrupted the unfavourable crystalline-amorphous Si core-shell structure typically seen in charge-cycled Si nanoparticle electrodes.[104] The best performance reported however, of a simple Si-MXene filtered composite, is that of the paper electrode fabricated by Tian *et al.* This electrode exhibited an initial capacity of 2930 mAh g^{-1} (at 0.2 A g^{-1} between 0.01–1.0 V), which is 1.4× or 60× more than either Si or $Ti_3C_2T_X$ alone, and showed excellent cycling stability and rate performance (Figure 5a–c). Even with a simple fabrication process, this work shows that MXenes are able to synergistically enhance Si by providing fast conduction pathways and facilitating volume expansion, while Si increases the Li capacity of the MXene by more than an order of magnitude.[105]

A more intricate composite – N-doped Ti_3C_2/Si@SiO_X@C – was fabricated by Zhang *et al.* using a combination of the Stöber method, magnesiothermic reduction, and carbonation. This composite had suitable conductivity to perform at high rates, and *ex situ* X-ray diffraction (XRD) analysis found that the MXene interlayer spacing was able to expand and contract with cycling, and thus facilitate the expansion of Si; after 1000 cycles at 10 C the electrode only swelled to 1.12× its original thickness. By contrast, commercial Si/C swelled 1.54×, causing it to flake away from the current collector. A full-cell was also fabricated with a $Li[Ni_{0.6}Co_{0.2}Mn_{0.2}]O_2$ cathode, which was flexible, stable with cycling, and had 2.8× the energy density of the best commercial Li-ion batteries available at the time of publishing (Figure 5d–g).[107]

3. Other Metal-Ion Batteries

Due to its rarity the current dominance of lithium-ion in the battery market is unsustainable, leading to research into the use of alternative metal ions.[97,110] For example, Mg^{2+} is 600× more abundant in the Earth's upper continental crust than Li^+,[97] and does not form dendrites during cycling. Multivalent ions, such as Mg^{2+} and Al^{3+} are also theoretically able to reach higher capacities than Li^+ due to their greater charge. The main issues which currently face these kinds of battery are longer charge times due to low diffusion rates, and poor cycling stability due to irreversible reactions and unstable electrolytes. Compared to other layered materials such as graphite, MXenes have very wide interlayer spacing which not only allows them to electrochemically intercalate large ions, but also to do so at a higher rate.[111,112]

3.1. Monovalent Ions: Na-ion and K-ion Batteries

Although they are some of the largest monatomic ions (and therefore the least mobile and hardest to intercalate), Na^+ and K^+ are well researched because of their similar chemistry to Li^+. Due to their lower charge:mass ratio, the theoretical gravimetric capacities of sodium and potassium are lower,[24,36,113] but their relative abundances in the Earth's upper continental crust are respectively 1100× and 1300× greater than lithium, and both are also abundant in seawater, making them cheap, apolitical resources.[97,114] Anodes for Na-ion batteries with high capacities and cycle lifetimes have been made from 2D nanomaterials such as phosphorus-doped graphene[115] and boron-doped rGO,[116] but a combination of high specific power and capacity is lacking. High rate capability is expected when MXenes are used, as Na^+ and K^+ ions are able to intercalate relatively quickly due to lower diffusion barriers, forming a mixture of mono- and bilayers *via* redox chemistry with the surface.[117–120] This intercalation expands the interlayer spacing of $Ti_3C_2T_X$, but shrinks the in-plane lattice parameters,[120,121] macroscopically distorting the electrode but also allowing ions to reach deeper adsorption sites and move more rapidly as the battery approaches full charge.[19] The maximum theoretical capacity of sodium ions on MXene ranges between 288 and 564 mAh g^{-1} (*cf.* Li on graphite: 372 mAh g^{-1})[122] depending on the MXene in question and the presence of OH or F groups, which inhibit both diffusion and adsorption.[23,24,36,123]

In 2017, Na- and Li-ion batteries using $Hf_3C_2T_X$ electrodes were compared, and while the Na-ion battery was more reliably cycled, it had less than half the capacity of the equivalent Li-ion set-up. Examination of the cycling behaviour also suggested that the Li^+ ions were able to progressively open up more adsorption sites, as well as oxidise surface groups forming an SEI which extended the cycle life.[45] The greater number of electrons in Na^+ and K^+ ions compared to Li^+ makes them more sensitive to electrostatic repulsion forces within the MXene. For example, Ti_3CNT_X was found to perform similarly to $Hf_3C_2T_X$ with Na^+, and with a higher capacity than $Ti_3C_2T_X$ due to the less homogeneous spatial distribution of electrons in the carbonitride layer enabling stronger adsorption of K^+ to the metal.[124] This also extends to the electron density of surface functional groups, to which the theoretical capacities of K-ion and Na-ion are more sensitive than that of Li-ion. In fact, unlike Li-ion or K-ion, the highest theoretical capacity for Na-ion electrodes has been found in O-terminated, rather than bare Ti_2C.[24,36] Computational studies have also predicted that replacing F and OH groups with Si, P or S will improve the capacity of Na-ion batteries.[125] Experimentally, only S-doped $Ti_3C_2T_X$ has been tested, and S was believed to displace C (not OH or F) in the crystal lattice. A high capacity of 114 mA g^{-1} was achieved by this method, and predominantly pseudocapa-

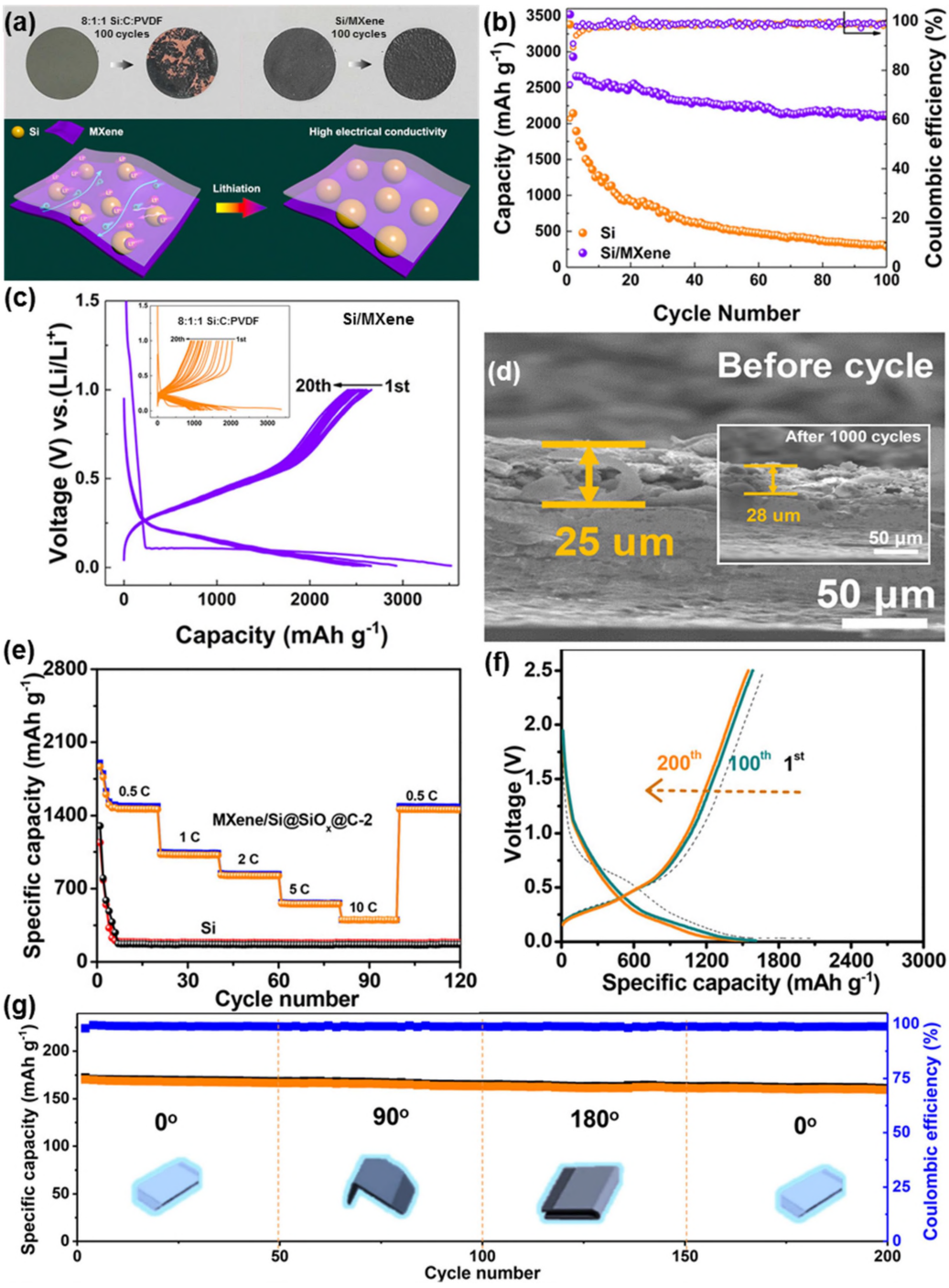

Figure 5. (a-c) Performance of Si/$Ti_3C_2T_X$ and Si/C electrodes produced by Tian *et al.* (a) Photographs of both electrodes before and after 100 charge-discharge cycles, and lithiation schematics of Si/$Ti_3C_2T_X$. (b) Cycling stability of Si/$Ti_3C_2T_X$ and Si/C electrodes at 200 mA g^{-1}. (c) Charge-discharge curves of Si/$Ti_3C_2T_X$ at 200 mA g^{-1} from 1st–20th cycles. Inset shows equivalent for Si/C.[105] (d–g) Performance of Ti_3C_2/Si@SiO_X@C electrode produced by Zhang *et al.* (d) Cross-sectional SEM images of Ti_3C_2/Si@SiO_X@C before and after (inset) 1000 cycles at 10 C. (e) Comparison of Ti_3C_2/Si@SiO_X@C Li capacity at various rates (0.5–10 C). (f) Charge-discharge profiles of Ti_3C_2/Si@SiO_X@C at 0.2 C from 1st, 100th and 200th cycles. (g) Cycling performance of Li-ion full-cell at 0.2 C under bending.[107] Reprinted (adapted) with permission from Refs. [105, 107]. Copyright 2019 American Chemical Society.

citive charge storage mechanisms were able to endow this electrode with excellent rate performance that was maintained after 2000 cycles.[126]

As with Li^+, TMO/MXene composites have also been found to improve the capacity of Na-ion batteries (Table 4); the most impressive of which so far published is a hierarchical Sb_2O_3/$Ti_3C_2T_X$ composite made by Guo *et al.*[127] This delivered 295–450 mAh g^{-1} at 0.2–2.0 A g^{-1}, and extended cycling gradually increased the capacity to 472 mAh g^{-1} at 0.1 A g^{-1}, suggesting the morphology may have been open enough for Na^+ ions to intercalate and open up new active sites as it cycles. However, analysis showed that as more active sites were gained the

Table 4. Summary of electrochemical performances of MXene-based electrodes in Na-ion cells.

Material	Ref.	Capacity/ mAh g^{-1}	Rate	Notes
$Ti_3C_2T_X$	[41]	79	0.2 A g^{-1}	Retained after 500 cycles
	[133]	178	0.2 A g^{-1}	
	[136]	101	0.1 A g^{-1}	
Ti_3C_2	[36]	351.8	–	Theoretical
$TiO_2/Ti_3C_2T_X$	[41]	101	0.2 A g^{-1}	Retained after 2000 cycles
Ti_3CNT_X	[124]	32	0.5 A g^{-1}	60% retained after 100 cycles
		90	10 mA g^{-1}	
$Hf_3C_2T_X$	[45]	68	50 mA g^{-1}	Retained after 200 cycles
		29	1.0 A g^{-1}	
Y_2C	[123]	564	N/A	Theoretical
S-doped $Ti_3C_2T_X$	[126]	114	4 A g^{-1}	Retained after 2000 cycles
		183	0.1 A g^{-1}	
$TiO_2@Ti_3C_2T_X$	[137]	220	30 mA g^{-1}	Retained after 5000 cycles
		116	0.96 A g^{-1}	
		70	3.84 A g^{-1}	
$CoNiO_2/Ti_3C_2T_X$	[138]	188	0.3 A g^{-1}	80% Retained after 140 cycles
		223	0.1 A g^{-1}	
$SnS/Ti_3C_2T_X$	[136]	256	1.0 A g^{-1}	Retained after 50 cycles
		413	0.1 A g^{-1}	
$Sb_2O_3/Ti_3C_2T_X$	[127]	295	2.0 A g^{-1}	97% retained after 100 cycles
		450	0.2 A g^{-1}	
DMSO/ $Ti_3C_2T_X$	[129]	120	0.1 A g^{-1}	85% Retained after 500 cycles
Crumpled $Ti_3C_2T_X$	[132]	120	0.5 A g^{-1}	Retained after 50 cycles
		250	20 mA g^{-1}	
$NaTi_{1.5}O_{8.3}$ nanoribbons	[133]	191	0.2 A g^{-1}	73% retained after 150 cycles
Alkalized $Ti_3C_2T_X$ nanoribbons	[17]	85	0.3 A g^{-1}	25% lost between 25th and 500th cycles
		167	20 mA g^{-1}	
Mo_2CT_X spheres	[19]	370	50 mA g^{-1}	Increased 38% after 1000 cycles at 0.5 A g^{-1}
		130	5 A g^{-1}	
$Ti_3C_2T_X$ spheres	[19]	330	50 mA g^{-1}	Increased 40% after 1000 cycles at 0.5 A g^{-1}
		124	5 A g^{-1}	
V_2CT_X spheres	[19]	340	50 mA g^{-1}	Increased 20% after 1000 cycles at 0.5 A g^{-1}
		174	5 A g^{-1}	
Lamellar $Ti_3C_2T_X$/rGO-cellulose	[139]	280	0.1 A g^{-1}	74% retained after 2000 cycles
		140	1.0 A g^{-1}	

electrode became more pseudocapacitive, and therefore the new sites were not equivalent to those originally being occupied.

Opening up 2D materials to improve ion access is important for large ions such as Na^+. Increasing *d*-spacing can improve rate, capacity and cyclability.[128] For instance, when HF-etched $Ti_3C_2T_X$ was intercalated with DMSO, as a Na-ion electrode it achieved a capacity of 120 mAh g^{-1} at 100 mA g^{-1}, retaining 86% after 500 cycles.[129] Taking this approach further, complete delamination *via* high-energy mechanical milling in DMSO enables the specific surface area of electrodes to be maximised. $Ti_3C_2T_X$ anodes produced *via* this method have delivered 267 mAh g^{-1} at 100 mA g^{-1} (73% retained after 500 cycles), and 150 mAh g^{-1} at 1 A g^{-1} (halved after 1500 cycles).[130] The cycle lifetime of these anodes needs to be improved by inhibiting the mechanism of flake restacking.

Barsoum,[131,132] and Dong,[17,133] *et al.* have demonstrated the use of morphological changes to inhibit flake restacking using ionic chemistry (Figure 6). Barsoum *et al.* investigated both acid-[132] and alkali-induced[131] crumpling of colloidal $Ti_3C_2T_X$ sheets to find that acid-crumpled MXene electrodes could demonstrate 250 mAh g^{-1} Na capacity, while alkali-crumpled electrodes maintained their capacity for 300 cycles. Dong *et al.*[17,133] mixed $Ti_3C_2T_X$ with KOH under ambient and oxidative hydrothermal conditions to make nanoribbons of alkalised $Ti_3C_2T_X$ (*a*-$Ti_3C_2T_X$) and $K_2Ti_4O_9$ respectively. Electrodes fabricated from these two materials showed quite similar electrochemical performance to each other, albeit the $K_2Ti_4O_9$ nanoribbons were consistently superior (Table 5). In K-ion half-cells, $K_2Ti_4O_9$ retained 75% of its capacity between cycles 100 and 900, whereas the *a*-$Ti_3C_2T_X$ only retained 70% between cycles 100

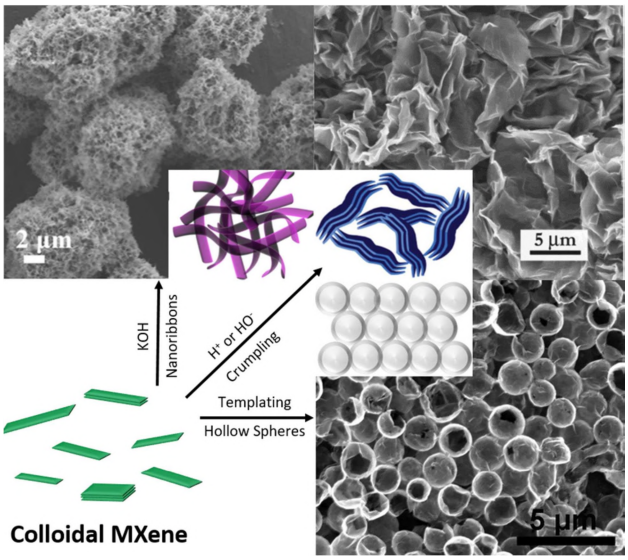

Figure 6. Schematic showing the formation of nanoribbons[17] (Copyright 2017 Elsevier), crumpled particles[132] (Copyright 2018 Taylor & Francis Group) and hollow spheres[19] (Copyright 2017 Wiley-VCH) from colloidal MXene, *via* shaking in 6 M KOH or dilute acid/alkali, or templating with sacrificial PMMA spheres.

Table 5. Summary of electrochemical performances of MXene-based electrodes in K-ion cells.

Material	Ref.	Capacity/ mAh g^{-1}	Rate	Notes
Ti_3C_2	[36]	191.8	–	Theoretical
Ti_2CO_2/ Graphene	[135]	209.80	–	Theoretical
V_2CO_2/ Graphene	[135]	207.22	–	Theoretical
Zr_2CO_2	[134]	474	–	Theoretical
$Zr_3C_2O_2$	[134]	326	–	Theoretical
Ti_3CNT_X	[124]	154	20 mA g^{-1}	75 mAh g^{-1} after 100 cycles
$K_2Ti_4O_9$ nanoribbons	[133]	88	0.3 A g^{-1}	51% retained after 900 cycles
		151	50 mA g^{-1}	
Alkalized $Ti_3C_2T_X$ nanoribbons	[17]	60	0.3 A g^{-1}	60% retained after 500 cycles
		141	20 mA g^{-1}	

and 500. The improved performance of $K_2Ti_4O_9$ was attributed in part to a more chemically and mechanically stable crystal structure with fewer OH functional groups (fluoride groups were not present in either electrode), and to the 3D porous structure of the long, thin, entangled nanoribbons, which enabled fast diffusion and high ion accessibility to almost all potential active sites.

An attempt to avoid the restacking of MXene sheets was made by Gogotsi *et al.*[19] in the production of hollow MXene spheres and 3D macroporous frameworks by PMMA-templating (Figure 6). 3D, macroporous films of $Ti_3C_2T_X$, V_2CT_X and Mo_2CT_X were fabricated by thermal evaporation of PMMA templates, and directly tested in Na-ion half cells, where they showed high capacities and non-diffusion-limited rates (Table 4). V_2CT_X gave the best performance on account of its wider interlayer spacing, and the capacities of all three MXene electrodes increased with cycling over the course of 1000 cycles at 2.5 C.

In summary, MXenes are able to accommodate Na^+ and K^+ ions where graphite cannot due to their wide interlayer spacing (*d*-spacing), and competitive theoretical capacities have been calculated.[23,24,36,123,134] However, full intercalation is in most cases diffusion-limited, and for this reason, efforts have been made to increase the *d*-spacing of MXenes. The most effective of these efforts (summarised in Tables 4 and 5) have been those which incorporate delaminated MXenes into a nanostructure which is specially designed to improve ion channels and prevent flake restacking, such as those of Gogotsi,[19] and Guo.[127] The strength of Gogotsi's PMMA-templated spheres lies in the specialised architecture and the wide *d*-spacing of V_2CT_X, while the high performance of Guo's hierarchical Sb_2O_3/$Ti_3C_2T_X$ electrodes can be attributed to it being a delaminated metal oxide composite. Further research could be done to combine these enhancements by making PMMA-templated spheres from metal oxide-anchored MXenes with very wide interlayer spacing, such as V_2CT_X or Y_2CT_X. Alternatively, the MXenes could be combined with graphene into heterostructures, which have been shown to have lower diffusion barriers to alkali metals than either MXene or graphene alone.[135]

3.2. Multivalent Ions: Mg-ion, Ca-ion and Al-ion Batteries

Mg^{2+} and Ca^{2+} ions have approximately twice the charge density of Na^+ or K^+, and are therefore able to attain approximately twice the theoretical gravimetric capacity.[24] It is for this reason, as well as their relative abundance[97] and moderate size, that magnesium and calcium are investigated as alternatives to lithium. However, higher charges reduce their diffusion constants about the anode surface[111] and risk making ion-electrode bonds irreversibly strong. These challenges may or may not ever be overcome by MXenes.

Despite being half as abundant in the Earth's upper continental crust as Na or K,[97] Mg^{2+} has a similar ionic radius to Li^+, twice the ionic charge, and is able to form bi- and tri-layers on a MXene surface, giving it some of the highest theoretical capacities ever calculated for MXene anodes (580-1050 mAh g^{-1}).[23,24] Alongside these high theoretical capacities, with regard to Ti_2C, intercalated Mg^{2+} is more thermodynamically stable than Li^+ or Na^+,[140] and when coupled with bare or O-terminated MXenes, predicted cell voltages fall in the range of 0.2–1.0 V.[23] However, as described in a number of reviews,[141–143] despite a century of electrochemical research,[144,145] Mg-ion batteries suffer difficulties attaining sufficiently reversible adsorption, fast ion diffusion, and stable electrolytes.[141,146,147] In light of this, efforts to develop high performance electrodes for Mg-ion batteries are greatly limited by the electrolytes available to researchers.

Magnesium metal is capable of acting as the anode in Mg-ion cells, and therefore electrode research has been dominated by the search for a cathode material. However, it is known that Mg metal forms a passivating (insulating) layer during charging, hindering cycling stability,[148] and thus some low voltage MXene cathodes in the literature might also be considered for application as anodes. For example, Yan *et al.* designed two types of MXene-based cathode for Mg-ion cells. The first was made using cetyltrimethylammonium bromide (CTAB) to increase the interlayer spacing of $Ti_3C_2T_X$ stacks,[149] and the second was made by hydrothermally compositing $Ti_3C_2T_X$ with MoS_2 (another suitable cathode material for Mg cells).[150] Both of these cathodes dramatically increased the amount of Mg^{2+} intercalated into $Ti_3C_2T_X$, with the pre-intercalation of CTAB/CTA^+ into delaminated $Ti_3C_2T_X$ achieving a capacity of 47–108 mAh g^{-1} at 50–2000 mA g^{-1}.[149] The $Ti_3C_2T_X/MoS_2$ composite exhibited a reasonable plateau in its galvanometric discharge curve, and delivered 93–165 mAh g^{-1} at 50–200 mA g^{-1}, but only retained 70 % of that after 50 cycles.[150]

Experimental work by Gogotsi *et al.* has found that the intercalation of smaller, higher charge cations contracts the interlayer spacing of $Ti_3C_2T_X$ MXene, while larger, lower charge cations increase interlayer spacing.[38] Therefore, in 2016, they used lithium and potassium ions synergistically with magnesium as both MXene pillars and co-charge carriers. The predicted effect was successfully measured, as cycling $Ti_3C_2T_X$ cathodes in K_2SO_4 electrolyte before switching to $MgSO_4$ increased the amount of intercalated Mg^{2+}, but also decreased the cell's coulombic efficiency, bringing it closer to that of a K-ion capacitor.[151] And in the case of lithium pillaring, a $Ti_3C_2T_X$/CNT composite electrode was able to deliver 40–105 mAh g^{-1} at 0.1–10 C, which was sustained over more than 500 cycles.[152]

Analogous to Mg-ion batteries are Ca-ion batteries, whose theoretical capacities with MXene anodes are *ca.* 300–500 mAh g^{-1} depending on the chemical composition of the MXene used.[24,36] Compared to Mg^{2+}, the Ca^{2+} ion is twice as abundant,[97] less polarisable,[153] and may attain better cycling stability due to a lower reduction potential.[154] However, very little work has been done to research Ca-ion batteries since the 1990's when it was decided that Ca plating may be impossible,[155,156] so there are no published examples of MXene-based Ca-ion batteries at the time of writing. In the last few years however, Ca-ion technology has made a resurgence since reversible Ca plating was achieved in 2016 by Ponrouch *et al.*,[157] and given the high theoretical capacity of Ca on MXenes, this is a worthy area of research for the community to pursue.[24]

Similarly to magnesium and calcium, aluminium is an abundant element (the most abundant metal in the Earth's upper continental crust)[97] which presents some key challenges to its implementation in rechargeable batteries. Aluminium is safer to handle, has a smaller ionic radius than Li^+, and its trivalency endows it with high theoretical capacity, but it has a large solvation shell in aqueous electrolyte and its trivalency often results in irreversible bonding and electrode fracture.[158] Al battery research is still in its early stages, but theoretical work predicts that Al^{3+} may exhibit a higher capacity on bare or O-terminated MXenes than any other ion previously tested.[24] These capacities were also calculated under the impression that Al could only cover 2/3rds of the MXene surface, but experimental work on multilayer $Ti_3C_2T_X$ indicates that a full monolayer is able to form, and alternating $Ti_3C_2T_X$ sheets will slide past each other to optimise the configuration.[117] Therefore, very high capacities are expected to be observed when Al cells are fabricated using MXenes, but it may be the case that the Al-MXene bonds in these cells will be too strong for reversible intercalation (especially considering the stability of $M_{n+1}AlC_n$ MAX phases).

The first published example of a MXene being used in an aluminium battery is the V_2CT_x cathode fabricated by Vahidmohammadi, *et al.*[159] When paired with an Al metal anode in ionic liquid electrolyte, this full cell is similar to the two-electrode half-cells used to test the majority of the reviewed Li-ion anodes (MXene working electrode, Li metal counter/reference electrode). However, this MXene is examined as a cathode due to the ability of Al metal to act as a safe, low-voltage anode in commercial applications (unlike Li metal). By partially delaminating the MXene and intercalating with tetrabutylammonium hydroxide (TBAOH), they achieved a very high discharge capacity and voltage of 300 $mAh\,g^{-1}$ and 1.2 V *vs.* Al/Al^{3+} at 100 $mA\,g^{-1}$. With reasonable rate performance and *ca.* 50% capacity retention after 100 cycles, this study presents one of the best intercalation-type Al battery cathodes to date, and warrants further research.

In conclusion, MXenes have very high theoretical capacities for Mg-, Ca- and Al-ion electrodes, but little progress has been made so far due to major issues in the wider field of multivalent metal-ion energy storage. Of the little experimental work which has been done, the greatest capacities observed are those of the $Ti_3C_2T_X/MoS_2$ and V_2CT_x cathodes for Mg^{2+} and Al^{3+} respectively, but even these require a significant amount of work before they are able to compete with Li-ion.[150,159] Given the high theoretical capacities and wide interlayer spacings of MXenes, they should remain a viable option for electrode materials as the fields of Mg-, Ca- and Al-ion battery research are developed.

4. The Effect of Microscale Morphology

When using 2D nanomaterials to fabricate macroscopic structures such as electrodes, the question naturally arises: how should one build into the third dimension? Most works have created thin film electrodes using simple methods such as filtration or slurry processing, but these traditional techniques will not necessarily lead to optimised electrodes. It was recently shown by Xia *et al.* that aligning MXene flakes along a chosen axis will increase ion diffusion in the direction parallel to said axis, and thus the output of fabricated supercapacitors can become thickness-independent up to *ca.* 200 μm.[160] To achieve similar improvements towards the development of thicker electrodes (which can achieve higher gravimetric and volumetric capacities), a number of 3D meso- and macroporous architectures for MXene-based battery anodes have been created. A selection of these is compared in Figure 7.

Meso- and macroporous anodes for Li-ion batteries include $NaO_{23}TiO_2/Ti_3C_2T_X$,[65] CNTs@Ti_3C_2,[89] MoS_2/Ti_3C_2@C,[77] $Ti_3C_2(OH)_2$ nanoribbons,[161] and a $Ti_3C_2T_X$/rGO foam.[85] The $NaO_{23}TiO_2/Ti_3C_2T_X$[65] and CNTs@Ti_3C_2[89] composites, which both bear a morphology reminiscent of a frieze carpet, show excellent rate performance and cycling stability, and this is attributed to the ability of the inter-flake $NaO_{23}TiO_2$ nanobelts and carbon nanotubes to provide a flexible, porous framework which shortens ion diffusion paths and reduces the effect of mechanical stress due to ion intercalation. This in turn is said to work synergistically with the large MXene flakes which provide highly conductive pathways for electron transport to the current collector. Now, while explanations of this kind seem perfectly reasonable, and these electrodes do indeed show good performance, there is currently insufficient data to test the ability of this explanation to quantitatively understand the improvements seen. For example, the proposal that improved rate performance is due to reduced ion diffusion resistance can be tested by examining the ease of ionic diffusion through the nanobelt/nanotube region. Huang *et al.* discussed the effect of extending the reaction time, which caused a greater density of $NaO_{23}TiO_2$ nanobelts to be observed, and an optimum reaction time of 100 hours was found. This fits with the notion that more densely packed nanobelts will negate the positive effect of widening inter-flake spacing, but the reduced performance is also attributed to agglomeration of nanobelts at these extended reaction times. Further, there is little evidence, in the electrochemical impedance data for example, that $NaO_{23}TiO_2$ nanobelt growth is aiding either Li^+ or Na^+ diffusion at all.[65]

The case is similar for the CNTs@Ti_3C_2 composites presented by Zheng *et al.*,[89] although in this case, comparison of these to a CNT/$Ti_3C_2T_X$ composite prepared by filtration of a mixed suspension[91] can help provide further insight into the effect of a frieze carpet-like morphology on electrochemical performance. CV profiles measured at similar rates show that the two composites exhibit a similar capacitive contribution, but have different redox behaviour. Both composites have delithiation peaks at *ca.* 1.8 V *vs.* Li/Li^+ (corresponding to reactions between Li and Ti), but that of the filtered composite is comparatively very broad, and so also a charge-discharge voltage plateau is only observed in the frieze carpet-like composite. Zheng *et al.* attribute their observed delithiation peaks to the oxidation of iron, which may occur preferentially to oxidation of titanium, allowing the redox peaks to remain sharp. The CNTs@Ti_3C_2 also demonstrate improved cycling and rate performance; the capacity is shown to significantly

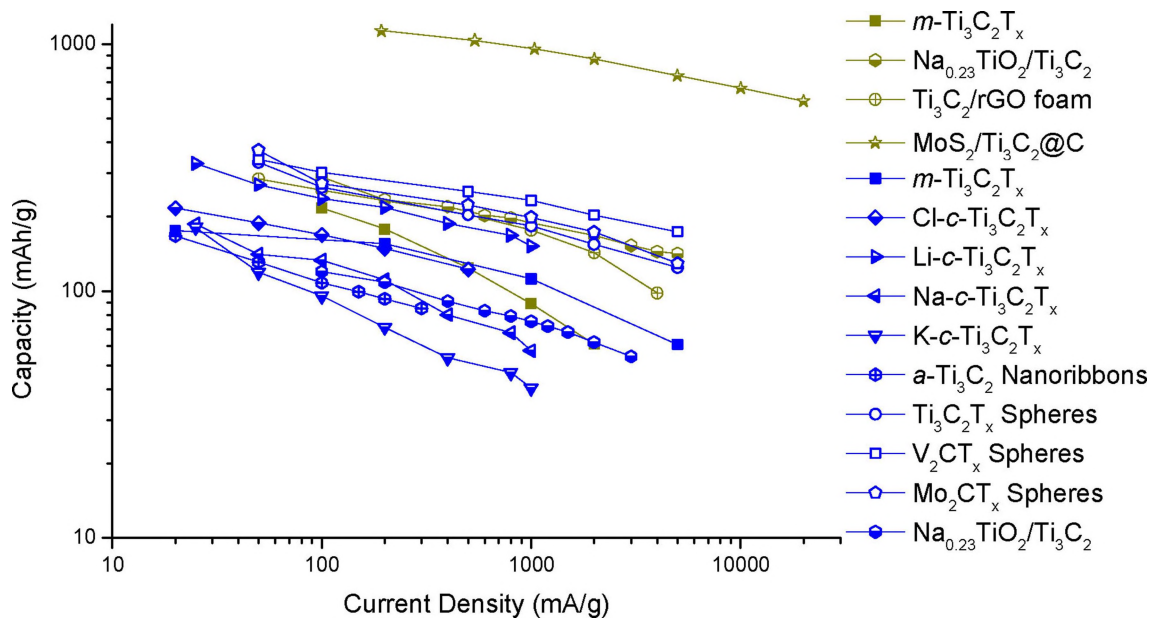

Figure 7. Current density *vs.* capacity of meso- and macroporous MXene-based anodes for Li-ion (yellow) and Na-ion (blue) batteries. The list includes multilayer $Ti_3C_2T_X$ (*m*-$Ti_3C_2T_X$),[19,41] $Na_{0.23}TiO_2/Ti_3C_2$,[65] Ti_3C_2/rGO foam,[85] MoS_2/Ti_3C_2@C,[77] crumpled $Ti_3C_2T_X$ (*c*-$Ti_3C_2T_X$) made by suspension in HCl,[132] LiOH, NaOH or KOH,[131] alkalised $Ti_3C_2T_X$ (*a*-Ti_3C_2) nanoribbons,[17] and hollow MXene spheres.[19]

increase with cycling, and remain relatively consistent upon switching between a range of discharge rates. By contrast, the filtered composite capacity increases less with cycling, and decreases several fold upon increasing the discharge rate by a smaller degree. A likely factor in this improvement is the high degree of connectivity between composite components (which is also highlighted in the MoS_2/Ti_3C_2@C composite), which improves electron transport and prevents composite breakdown during cycling. The types of enhancement observed in comparing the two CNT/MXene composites are not seen in MXene/iron composites,[68] and so it is fair to propose that the improved performance is due to the increased surface area and connectivity of the frieze carpet-like morphology, and not simply due to the presence of iron.

A conceptually simple way to increase the ion accessibility of any composite is to turn it in to a macroporous foam or foam-like structure. However, while the concept is very simple, the effect of microporosity on MXene anodes has not been thoroughly examined or quantified. For example, rGO/$Ti_3C_2T_X$ foams containing a variety of rGO:MXene mass ratios were compared by Ma *et al.*,[85] but while these foams did exhibit different nanoscale morphologies, the effects of these morphologies were not isolated from the effects of varying the chemical composition. In this case it is possible to compare the findings made by Ma *et al.* to those presented by Shen *et al.*[84] in their study of an rGO/$Ti_3C_2T_X$ thin film. It can clearly be seen in Figure 8 that the rGO/$Ti_3C_2T_X$ foam experiences different electrochemistry and exhibits superior gravimetric capacity and rate performance when compared to the rGO/$Ti_3C_2T_X$ thin film, and examination of the Nyquist plots given in the publications indicate that the foams exhibit lower ionic diffusion barriers. Unfortunately, because of a number of differences between their experimental procedures, this comparison alone cannot be used to draw any quantitative conclusions about morphological effects, and it is therefore important in future research for this to be analysed experimentally.

Research into carbon-based anodes for Na-ion batteries has shown that porous structures enhance their capacity through the facilitation of deep and facile intercalation.[162] In accordance with this reasoning, a number of the Na-ion and K-ion anodes discussed in this review have incorporated some kind of meso- or macroporous architecture.[17,19,131,132] One morphology that has been exploited a number of times for these anodes is that of nanoribbons (Figure 6), for example, in the works published by Zhang and Dong *et al.*[17,133,161] Again, the electrodes presented showed impressive capacity, rate performance, cycling stability, and even low deintercalation voltages, but the choice of focus in these studies does not allow for explicit elucidation of the benefits which arise from microporosity, and all of the electrochemical tests were in fact carried out in coin cells which compress the electrode and decrease the pore size. With that in mind, it is worth noting that Zhang *et al.* recorded a decreased Warburg impedance element (related to ion diffusion resistance) in their $Ti_3C_2(OH)_2$ nanoribbons,[161] and Dong *et al.* used gas sorption analysis to estimate the accessible surface area of alkalized $Ti_3C_2T_X$ nanoribbons to be 6.25× greater than that of MXene nanosheets.[17] Another key factor which was not thoroughly discussed is the effect of the conductive additives used, and microscopy should be used to investigate this. Although it is not a controlled experiment, Dong *et al.* have partially elucidated the effect of their novel nanoribbon structure by comparing the performance of their $K_2Ti_4O_9$ nanoribbons to similar $K_2Ti_4O_9$ nanoparticles and $K_2Ti_8O_{17}$ nanorods.[163,164] Although limited (just as the comparison presented in Figure 8), this comparison

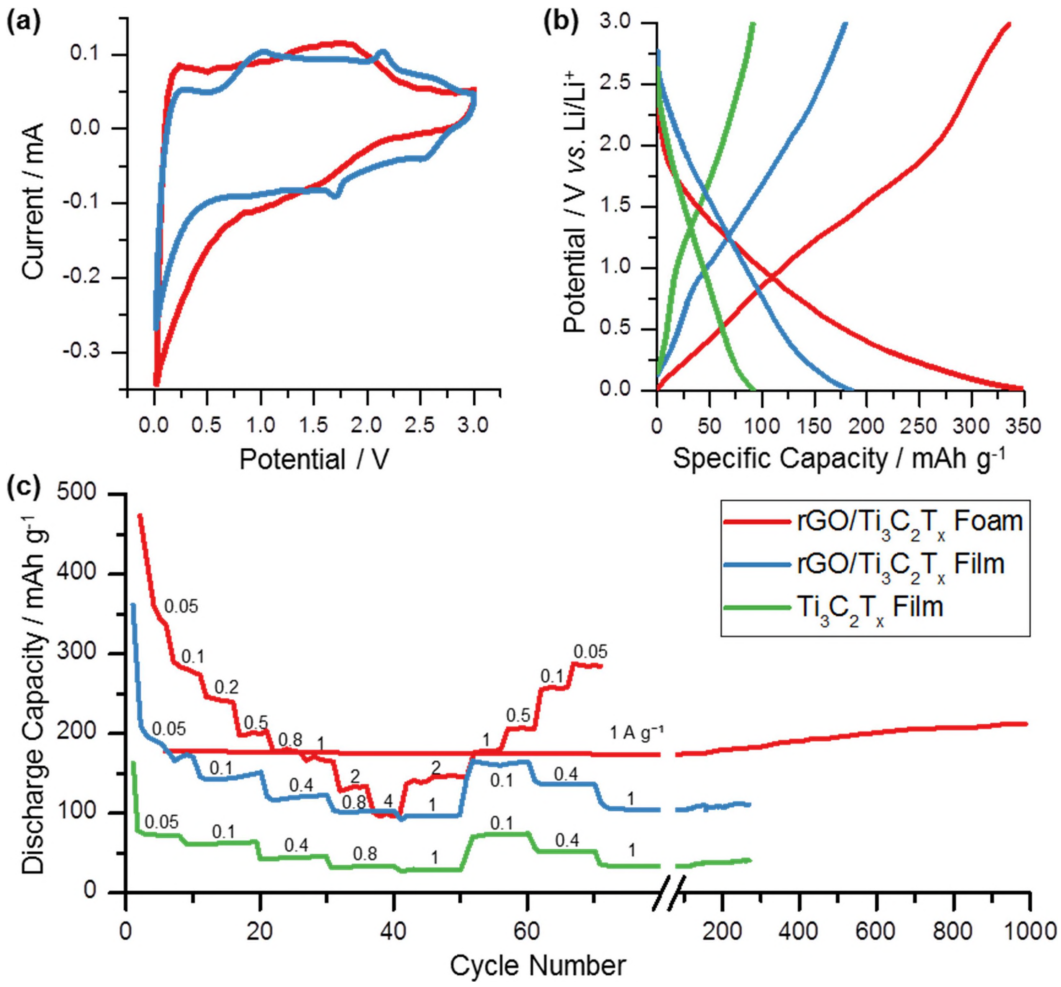

Figure 8. Electrochemical test results of an rGO/$Ti_3C_2T_X$ foam published by Ma *et al.*,[85] and an rGO/$Ti_3C_2T_X$ thin film published by Shen *et al.*[84] (a) Cyclic voltammetry profiles measured at 0.2 mV s^{-1}; (b) 50 mA g^{-1} charge-discharge curves of both the rGO/$Ti_3C_2T_X$ composites and a pristine $Ti_3C_2T_X$ sample fabricated by Shen *et al.*; (c) rate and cycling performances of the three materials shown in (b).

suggests the entangled nanoribbon structure may increase capacity by ca. 30 % and cyclability by more than 100 %.

After finding that compact $Ti_3C_2T_X$ flakes deliver lower capacity due to inhibited ion diffusion,[37,67] Barsoum *et al.* directly assessed the effect of porosity on electrode performance in their two-part study of crumpled MXene flocs, which were formed by the addition of strong acids and bases to aqueous colloids (Figure 6).[131,132] Although the half-cells tested were not optimised – as energy storage was not the main focus of the work – the authors were able to show that crumpling increases the Na capacity of delaminated $Ti_3C_2T_X$ electrodes approximately tenfold, and inserting Li increases it approximately twice as much again (Figure 9). The choice of base used for MXene crumpling (LiOH, NaOH or KOH) clearly had a significant effect on performance, as the alkali metal cation intercalates between MXene sheets and affects accessibility to Na^+. $Ti_3C_2T_X$ crumpled using LiOH (3D Li-*c*-$Ti_3C_2T_X$ in Figure 9), for example, initially exhibited one of the highest gravimetric capacities ever found in a MXene-based Na-ion electrode, but (for currently unknown reasons) it exhibited much worse cycling stability than either 3D Na-*c*-$Ti_3C_2T_X$ or 3D K-*c*-$Ti_3C_2T_X$. Both of these, on the other hand, were found to only slightly improve upon the capacity of multilayer $Ti_3C_2T_X$ (to the point where there is negligible difference at higher current rates), but they did improve the cycling stability – 3D Na-*c*-$Ti_3C_2T_X$ was found to maintain its initial reversible capacity after 1000 cycles at 1.5 A g^{-1}. This is believed to be because of the pillaring effect of large cations working synergistically with the porosity effect of crumpling to reduce intercalative volume changes.

These morphology-driven improvements are certainly promising, and they demonstrate the importance of considering the way MXene sheets assemble during electrode preparation. But as with any parameter under consideration, it is important to find a balance between the positive and negative effects of increasing 3D porosity. While the opening up of MXene structures may improve ionic conductivity (especially in thick electrodes), it will inevitably have a negative effect on both electronic conductivity and volumetric capacity. Figure 9a shows the improvement Natu *et al.*[132] made to electrode performance by adding 20 wt% carbon black, which was necessary due to the decreased connectivity between crumpled MXene flakes, and although the relevant data was not

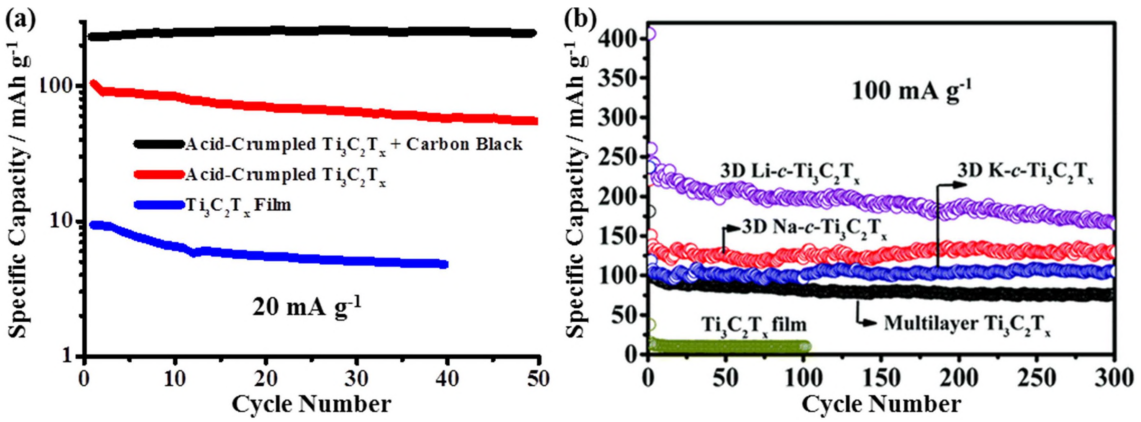

Figure 9. Cycling performances of Na-ion half-cells. (a) Acid-crumpled $Ti_3C_2T_X$ (foam-like) and a filtered $Ti_3C_2T_X$ film; produced from data presented by Natu *et al.*[132] (b) Filtered $Ti_3C_2T_X$ film, multilayer $Ti_3C_2T_X$, and $Ti_3C_2T_X$ which has been crumpled (*c*-$Ti_3C_2T_X$) using LiOH, NaOH, or KOH.[131] Copyright 2018 Royal Society of Chemistry.

published, it can safely be assumed that electrodes fabricated from porous MXene structures contain less active material per unit volume, and therefore exhibit lower volumetric capacities. That being said, most of the papers discussed in this section have presented reasonable values of areal mass loading (*ca.* 1 mg cm^{-2}), and given the compression forces within a coin cell, these should also correspond to reasonable volumetric mass loadings. The effect this compression has had on porosity is not reported, but it is likely to be insignificant, as the highest Na-ion capacity ever recorded for pure $Ti_3C_2T_X$ was that of highly porous, hollow MXene spheres (Figure 6) under compression in a coin cell (295 mAh g^{-1} at 0.5 A g^{-1}).[19] Therefore, while porosity in electrodes has the potential to enhance both rate and cycling performance, it is likely that the pores do not need to be of much volume before additional porosity has a negligible effect.

5. Hybrid Ion Capacitors

Before the end of this review, it is worth a short discussion of how MXenes have so far been used as anodes in hybrid ion capacitors. Conceptually, hybrid ion capacitors (HICs) are asymmetrical supercapacitors where one electrode is that typical of a supercapacitor, storing energy through electrical double layer capacitance (EDLC), and the other is redox-active, as in a battery. Modern HICs usually combine these electrodes using an organic electrolyte which can sustain a high voltage, giving them more similarity to Li-ion batteries.[165] As discussed in a review by Ding *et al.*, HICs presently serve to compete with ELDC supercapacitors in applications where higher specific energy takes priority over cyclability.[166]

Owing to their pseudocapacitive characteristics, a number of MXene-based anodes have been used for Li-ion and Na-ion hybrid capacitors, such as those in early works by Come, Wang *et al.*[167,168] Pioneering research by Come *et al.* paired a Ti_2CT_x anode with an activated carbon cathode to make a Li-ion capacitor which delivered a maximum power of 190 kW kg^{-1}, and stored a maximum of 50 Wh kg^{-1}, retaining *ca.* 85% of its initial capacity after 1000 cycles.[168] A Na-ion hybrid capacitor later developed by Wang *et al.* also utilised a Ti_2CT_x anode, but paired it with a $Na_2Fe_2(SO_4)_3$ cathode, delivering 2.4 V and 90–40 mAh g^{-1} at 1.0–5.0 A g^{-1}. As in MXene-based batteries, the first charge-discharge cycle had a very low coulombic efficiency (presumably due to SEI formation), but between the 2nd and 100th cycles at 0.6 A g^{-1}, 96% of its capacity was retained.[167] These, as well as other MXenes, perform well compared to a number of other anode materials – especially at high current rates – but when tested at lower power, they currently only reach half the energy density of the best carbon-based HIC electrodes.[165,166,169,170] Like batteries, these anodes could benefit from shallower gradients in their charge-discharge curves, as this signifies an increased capacity within the voltage window available. However, unlike in batteries, completely flat voltage plateaus are not necessary, which may be more suitable and achievable for MXenes, as sharp redox peaks are generally only seen when MXenes are composited with materials such as Fe_2O_3, which exhibit worse cycling degradation and capacity retention.[171]

As far as the authors of this review are aware, none of the MXene-containing HICs presented in the literature have been tested in extremely long cycle tests (e.g., >50k cycles) which other HICs and conventional supercapacitors are subjected to. It is important for this aspect of MXene HIC research to progress, as the applications which currently use supercapacitors expect to see little capacity degradation over these extreme cycling periods. A significant improvement may be gained (in battery research as well) with further insights into the SEI layer of MXenes, as the first charge-discharge cycle of any MXene redox system will demonstrate that there are energetic, irreversible processes taking place. Progress in understanding and utilisation of these processes may allow MXene-based HICs to achieve cyclabilities comparable to EDLC supercapacitors.

High power applications raise the priority of having good accessibility of ions to active sites, which is why composites and 3D porous architectures may also be useful for improving the lifetimes of MXene HIC electrodes. For example, a simple

$Ti_3C_2T_x$/CNTs composite fabricated by Yu *et al.* retained 81 % of its initial capacity for 5000 cycles at 2 $A g^{-1}$,[172] and a V_2C MXene pillared using covalently bound Co delivered a capacity of 1117 $mAh g^{-1}$ at 0.1 $A g^{-1}$, and maintained a capacity of 250 $mAh g^{-1}$ at 8 $A g^{-1}$ for 15000 cycles.[173] Both of these high performance examples are Li-ion HICs, but it has been found that Na-ion HICs are not generally inferior to Li-ion in the same way that batteries are (although the reason for this is uncertain). So researchers should focus on developing Na-ion HICs, as these provide a more sustainable solution to the world's energy storage problems.[166]

6. Summary and Outlook

Since the initial discovery of MXenes in 2011, anodes based on these materials have been developed for metal-ion batteries using a variety of composites and nanoscale morphologies. With qualities such as wide interlayer spacing, MXenes are able to facilitate fast ion diffusion and large volume expansions, and also intercalate large ions such as Na^+ and K^+ for "beyond lithium-ion" batteries. Bare and O-terminated MXenes typically give the best electrochemical performance with any metal ion, and while bare MXenes appear to be practically unattainable, O-terminated MXenes (which can also be used as a substrate to grow dendrite-free Li metal anodes)[39] should become more common as fluorine-free syntheses are developed and employed.

According to the classification system set out by Eftekhari,[20] MXene-based anodes are typically pseudocapacitive with a wide voltage window, and as such the charge-discharge curves of half-cells are almost always heavily sloped. This is important, not only because it makes them appropriate for use in hybrid ion capacitors, but also because it can lead to inappropriate interpretation of performance data, such that MXene anodes in full Li-ion cells would not be able to deliver as high a voltage as graphite anodes do presently (although it is worth noting that not many full cells have actually been tested). Some MXene composites reviewed here have shown voltage plateaus due to the discreet redox potentials exhibited by their partner materials, but MXenes are also known to experience a rapid drop in capacity after a few charge-discharge cycles, so deeper understanding of the mechanisms behind this might lead to the development of specially functionalised MXenes with discreet, reversible redox potentials.

Because MXenes are both denser and more expensive than graphite due to the presence of transition metals, they show their greatest potential for Li-ion batteries when they are able to act as a flexible, conductive scaffold or multifunctional binder for other materials which are capable of achieving much higher capacities but are normally unable to display high rate performance or long-term cycling stability. The greatest advantages appear to be in cases where the unique chemistry of MXenes is exploited for both facile material synthesis and strong interconnectivity of composite components (as in the case of partially oxidised MXenes such as TiO_2@$Ti_3C_2T_x$ and $Li_4Ti_5O_{12}$/$Ti_3C_2T_X$),[56,64] or where the tunable interlayer spacing of MXenes is able to facilitate large volume expansions (such as in Ti_3C_2/Si@SiO_X@C).[107]

To fully exploit the entire MXene sheet, sufficient interlayer space must be provided for metal plating, and the intercalation barrier of deep adsorption sites must be lowered (especially in the case of large Na^+ and K^+ ions) by either delamination or expansion of the interlayer spacing (i.e., pillaring). Interlayer expansion and delamination is easily achieved *in situ* during MAX phase etching by LiF/HCl solution, but it has also been demonstrated in HF-etched MXenes through intercalation of molecules and larger ions such as DMSO and K^+.[37,38,149,151] Restacking can be prevented by thoroughly homogenising the components in MXene composites, or by the fabrication of a 3D meso- or macroporous design. Now, while the exploitation of porous structures has certainly proven effective to increase capacity,[19] there is a large gap in our understanding of the effects of pore size, shape, and spatial frequency, and development in this area is key to our ability to balance the benefits of added porosity with the resulting loss of volumetric capacity and electronic conductivity. As developments are made in the printing of MXenes, it may even be possible to study these microstructures in tandem with the effects of changing the macroscopic morphology of MXene electrodes.[39,174–176]

Finally, an outstanding problem for the implementation of MXenes in any commercial product is their fast oxidation. Since this is also related to the selection of functional groups on the surface of MXenes, it stands to reason that more research should expand upon the work set out by Wu *et al.*[77] to synthesise MXenes with functionalities that are not only electrochemically advantageous, but also resist irreversible oxidative processes. This is especially true for the development of "beyond lithium-ion" batteries which are more sensitive to the distribution of electron density on the surface of electrodes, and therefore stand to gain the most benefit from an optimised MXene surface.

Acknowledgements

This work was written by M.G. under the supervision of S.B. and M.B., and is supported by the Graphene NOWNANO CDT, funded through EPSRC grant (EP/L01548X/1). S.B. would also like to acknowledge Heilongjiang Huasheng Graphite Co. Ltd.

[1] A. Elmarakbi, W. L. Azoti, *10th Int. Conf. Compos. Sci. Technol.* **2015**, 1,4.
[2] D. Larcher, J.-M. Tarascon, *Nat. Chem.* **2015**, *7*, 19.
[3] S. Chu, Y. Cui, N. Liu, *Nat. Mater.* **2017**, *16*, 16.
[4] L. Verger, C. Xu, V. Natu, H.-M. Cheng, W. Ren, M. W. Barsoum, *Curr. Opin. Solid State Mater. Sci.* **2019**, *23*, 149.
[5] Y. Gogotsi, R. M. Penner, *ACS Nano* **2018**, *12*, 2081.
[6] A. Noori, M. F. El-Kady, M. S. Rahmanifar, R. B. Kaner, M. F. Mousavi, *Chem. Soc. Rev.* **2019**, *48*, 1272.
[7] B.-M. M. Jun, S. Kim, J. Heo, C. M. Park, N. Her, M. Jang, Y. Huang, J. Han, Y. Yoon, *Nano Res.* **2019**, *12*, 471.

[8] J. Pang, R. G. Mendes, A. Bachmatiuk, L. Zhao, H. Q. Ta, T. Gemming, H. Liu, Z. Liu, M. H. Rummeli, *Chem. Soc. Rev.* **2019**, *48*, 72.
[9] J. Yang, W. Bao, P. Jaumaux, S. Zhang, C. Wang, G. Wang, *Adv. Mater. Interfaces* **2019**, *6*, 1802004.
[10] S. Sun, C. Liao, A. M. Hafez, H. Zhu, S. Wu, *Chem. Eng. J.* **2018**, *338*, 27.
[11] X. Zhang, Z. Zhang, Z. Zhou, *J. Energy Chem.* **2018**, *27*, 73.
[12] D. Xiong, X. Li, Z. Bai, S. Lu, *Small* **2018**, *14*, 1703419.
[13] J. M. Tarascon, M. Armand, *Nature* **2001**, *414*, 359.
[14] N. Nitta, F. Wu, J. T. Lee, G. Yushin, *Mater. Today* **2015**, *18*, 252.
[15] M. Naguib, M. Kurtoglu, V. Presser, J. Lu, J. Niu, M. Heon, L. Hultman, Y. Gogotsi, M. W. Barsoum, *Adv. Mater.* **2011**, *23*, 4248.
[16] T.-H. Park, J.-S. Yeo, M.-H. Seo, J. Miyawaki, I. Mochida, S.-H. Yoon, *Electrochim. Acta* **2013**, *93*, 236.
[17] P. Lian, Y. Dong, Z.-S. S. Wu, S. Zheng, S. Wang, C. Sun, J. Qin, X. Shi, X. Bao, X. Wang, Sen Wang, C. Sun, J. Qin, X. Shi, X. Bao, S. Wang, C. Sun, J. Qin, X. Shi, X. Bao, *Nano Energy* **2017**, *40*, 1.
[18] P. Simon, *ACS Nano* **2017**, *11*, 2393.
[19] M.-Q. Zhao, X. Xie, C. E. Ren, T. Makaryan, B. Anasori, G. Wang, Y. Gogotsi, *Adv. Mater.* **2017**, *29*, 1702410.
[20] A. Eftekhari, *Energy Storage Mater.* **2017**, *7*, 157.
[21] Y. Dall'Agnese, M. R. Lukatskaya, K. M. Cook, P.-L. Taberna, Y. Gogotsi, P. Simon, *Electrochem. Commun.* **2014**, *48*, 118.
[22] J. Li, X. Yuan, C. Lin, Y. Yang, L. Xu, X. Du, J. Xie, J. Lin, J. Sun, *Adv. Energy Mater.* **2017**, *7*, 1602725.
[23] C. Eames, M. S. Islam, *J. Am. Chem. Soc.* **2014**, *136*, 16270.
[24] Y. Xie, Y. Dall'Agnese, M. Naguib, Y. Gogotsi, M. W. Barsoum, H. L. Zhuang, P. R. C. Kent, *ACS Nano* **2014**, *8*, 9606.
[25] Y. Xie, M. Naguib, V. N. Mochalin, M. W. Barsoum, Y. Gogotsi, X. Yu, K. W. Nam, X. Q. Yang, A. I. Kolesnikov, P. R. C. Kent, *J. Am. Chem. Soc.* **2014**, *136*, 6385.
[26] Q. Tang, Z. Zhou, P. Shen, *J. Am. Chem. Soc.* **2012**, *134*, 16909.
[27] R. Ibragimova, M. J. Puska, H.-P. Komsa, *ACS Nano* **2019**, *13*, 9171.
[28] K. Fan, Y. Ying, X. Li, X. Luo, H. Huang, *J. Phys. Chem. C* **2019**, *123*, 18207.
[29] J. Zhu, U. Schwingenschlögl, *2D Mater.* **2017**, *4*, 025073.
[30] T. Li, X. Yan, L. Huang, J. Li, L. Yao, Q. Zhu, W. Wang, W. Abbas, R. Naz, J. Gu, Q. Liu, W. Zhang, D. Zhang, *J. Mater. Chem. A* **2019**, DOI 10.1039/C9TA03254A.
[31] X. Yu, X. Cai, H. Cui, S. W. Lee, X. F. Yu, B. Liu, *Nanoscale* **2017**, *9*, 17859.
[32] S. Yang, P. Zhang, F. Wang, A. G. Ricciardulli, M. R. Lohe, P. W. M. Blom, X. Feng, *Angew. Chem.* **2018**, *57*, 15491.
[33] T. Li, L. Yao, Q. Liu, J. Gu, R. Luo, J. Li, X. Yan, W. Wang, P. Liu, B. Chen, W. Zhang, W. Abbas, R. Naz, D. Zhang, *Angew. Chem. Int. Ed.* **2018**, *57*, 6115.
[34] W. Sun, S. A. Shah, Y. Chen, Z. Tan, H. Gao, T. Habib, M. Radovic, M. J. Green, *J. Mater. Chem. A* **2017**, *5*, 21663.
[35] C. J. Zhang, S. Pinilla, N. McEvoy, C. P. Cullen, B. Anasori, E. Long, S. H. Park, A. Seral-Ascaso, A. Shmeliov, D. Krishnan, C. Morant, X. Liu, G. S. Duesberg, Y. Gogotsi, V. Nicolosi, *Chem. Mater.* **2017**, *29*, 4848.
[36] D. Er, J. Li, M. Naguib, Y. Gogotsi, V. B. Shenoy, *ACS Appl. Mater. Interfaces* **2014**, *6*, 11173.
[37] O. Mashtalir, M. Naguib, V. N. Mochalin, Y. Dall'Agnese, M. Heon, M. W. Barsoum, Y. Gogotsi, *Nat. Commun.* **2013**, *4*, 1716.
[38] M. D. Levi, M. R. Lukatskaya, S. Sigalov, M. Beidaghi, N. Shpigel, L. Daikhin, D. Aurbach, M. W. Barsoum, Y. Gogotsi, *Adv. Energy Mater.* **2015**, *5*, 1400815.
[39] K. Shen, B. Li, S. Yang, *Energy Storage Mater.* **2019**, DOI 10.1016/j.ensm.2019.08.015.
[40] S. J. Kim, M. Naguib, M. Zhao, C. Zhang, H.-T. Jung, M. W. Barsoum, Y. Gogotsi, *Electrochim. Acta* **2015**, *163*, 246.
[41] C. Yang, Y. Liu, X. Sun, Y. Zhang, L. Hou, Q. Zhang, C. Yuan, *Electrochim. Acta* **2018**, *271*, 165.
[42] D. Sun, M. Wang, Z. Li, G. Fan, L. Z. Fan, A. Zhou, *Electrochem. Commun.* **2014**, *47*, 80.
[43] M. Naguib, J. Come, B. Dyatkin, V. Presser, P. L. Taberna, P. Simon, M. W. Barsoum, Y. Gogotsi, *Electrochem. Commun.* **2012**, *16*, 61.
[44] F. Du, H. Tang, L. Pan, T. Zhang, H. Lu, J. Xiong, J. Yang, C. (John) Zhang, *Electrochim. Acta* **2017**, *235*, 690.
[45] J. Zhou, X. Zha, X. Zhou, F. Chen, G. Gao, S. Wang, C. Shen, T. Chen, C. Zhi, P. Eklund, S. Du, J. Xue, W. Shi, Z. Chai, Q. Huang, *ACS Nano* **2017**, *11*, 3841.
[46] M. Naguib, J. Halim, J. Lu, K. M. Cook, L. Hultman, Y. Gogotsi, M. W. Barsoum, *J. Am. Chem. Soc.* **2013**, *135*, 15966.
[47] S. Zhao, X. Meng, K. Zhu, F. Du, G. Chen, Y. Wei, Y. Gogotsi, Y. Gao, *Energy Storage Mater.* **2017**, *8*, 42.
[48] L. Wang, H. Guo, W. Wang, K. Teng, Z. Xu, C. Chen, C. Li, C. Yang, C. Hu, *Electrochim. Acta* **2016**, *211*, 499.
[49] J. Xu, S. Gu, L. Fan, P. Xu, B. Lu, *Electrochim. Acta* **2016**, *196*, 125.
[50] L. Lin, Q. Pan, *J. Mater. Chem. A* **2015**, *3*, 1724.
[51] Y. Zhang, Y. Wei, H. Li, Y. Zhao, F. Yin, X. Wang, *Mater. Lett.* **2016**, *184*, 235.
[52] J. Lin, J. He, Y. Chen, Q. Li, B. Yu, C. Xu, W. Zhang, *Electrochim. Acta* **2016**, *215*, 667.
[53] S. Fang, L. Shen, H. Zheng, X. Zhang, *J. Mater. Chem. A* **2015**, *3*, 1498.
[54] M. Naguib, O. Mashtalir, M. R. Lukatskaya, B. Dyatkin, C. Zhang, V. Presser, Y. Gogotsi, M. W. Barsoum, *Chem. Commun.* **2014**, *50*, 7420.
[55] B. Ahmed, D. H. Anjum, M. N. Hedhili, Y. Gogotsi, H. N. Alshareef, *Nanoscale* **2016**, *8*, 7580.
[56] C. J. (John) Zhang, S. J. Kim, M. Ghidiu, M.-Q. Zhao, M. W. Barsoum, V. Nicolosi, Y. Gogotsi, *Adv. Funct. Mater.* **2016**, *26*, 4143.
[57] A. Byeon, C. B. Hatter, J. H. Park, C. W. Ahn, Y. Gogotsi, J. W. Lee, *Electrochim. Acta* **2017**, *258*, 979.
[58] C. Zhang, M. Beidaghi, M. Naguib, M. R. Lukatskaya, M. Q. Zhao, B. Dyatkin, K. M. Cook, S. J. Kim, B. Eng, X. Xiao, D. Long, W. Qiao, B. Dunn, Y. Gogotsi, *Chem. Mater.* **2016**, *28*, 3937.
[59] T. Habib, X. Zhao, S. A. Shah, Y. Chen, W. Sun, H. An, J. L. Lutkenhaus, M. Radovic, M. J. Green, *NPJ 2D Mater. Appl.* **2019**, *3*, 8.
[60] R. Lotfi, M. Naguib, D. E. Yilmaz, J. Nanda, A. C. T. Van Duin, *J. Mater. Chem. A* **2018**, *6*, 12733.
[61] Y. Chae, S. J. Kim, S. Y. Cho, J. Choi, K. Maleski, B. J. Lee, H. T. Jung, Y. Gogotsi, Y. Lee, C. W. Ahn, *Nanoscale* **2019**, *11*, 8387.
[62] S. Huang, V. N. Mochalin, *Inorg. Chem.* **2019**, *58*, 1958.
[63] W. L. Zhang, W. Wei, W. Liu, T. Guan, Y. Tian, H. Zeng, *Chem. Eng. J.* **2019**, *378*, 122170.
[64] J. Wang, S. Dong, H. Li, Z. Chen, S. Jiang, L. Wu, X. Zhang, *J. Electroanal. Chem.* **2018**, *810*, 27.
[65] J. Huang, R. Meng, L. Zu, Z. Wang, N. Feng, Z. Yang, Y. Yu, J. Yang, *Nano Energy* **2018**, *46*, 20.
[66] Y. Xu, D. Bauer, M. Lübke, T. E. Ashton, Y. Zong, J. A. Darr, *J. Power Sources* **2018**, *408*, 28.
[67] M.-Q. Zhao, M. Torelli, C. E. Ren, M. Ghidiu, Z. Ling, B. Anasori, M. W. Barsoum, Y. Gogotsi, *Nano Energy* **2016**, *30*, 603.
[68] Y. Wang, Y. Li, Z. Qiu, X. Wu, P. Zhou, T. Zhou, J. Zhao, Z. Miao, J. Zhou, S. Zhuo, *J. Mater. Chem. A* **2018**, *6*, 11189.
[69] F. Yu, X. Wang, R. Du, F. Jiang, Y. Zhou, *Mater. Lett.* **2019**, *253*, 162.
[70] M. Lu, H. Li, W. Han, Y. Wang, W. Shi, J. Wang, H. Chen, H. Li, B. Zhang, W. Zhang, W. Zheng, *Nanoscale* **2019**, *11*, 15037.
[71] J. Luo, X. Tao, J. Zhang, Y. Xia, H. Huang, L. Zhang, Y. Gan, C. Liang, W. Zhang, *ACS Nano* **2016**, *10*, 2491.
[72] F. Wang, Z. Wang, J. Zhu, H. Yang, X. Chen, L. Wang, C. Yang, *J. Mater. Sci.* **2017**, *52*, 3556.
[73] B. Ahmed, D. H. Anjum, Y. Gogotsi, H. N. Alshareef, *Nano Energy* **2017**, *34*, 249.
[74] Y. T. Liu, P. Zhang, N. Sun, B. Anasori, Q. Z. Zhu, H. Liu, Y. Gogotsi, B. Xu, *Adv. Mater.* **2018**, *30*, 1707334.
[75] M. Zheng, R. Guo, Z. Liu, B. Wang, L. Meng, F. Li, T. Li, Y. Luo, *J. Alloys Compd.* **2018**, *735*, 1262.
[76] C. Chen, X. Xie, B. Anasori, A. Sarycheva, T. Makaryan, M. Zhao, P. Urbankowski, L. Miao, J. Jiang, Y. Gogotsi, *Angew. Chem. Int. Ed.* **2018**, *57*, 1846.
[77] X. Wu, Z. Wang, M. Yu, L. Xiu, J. Qiu, *Adv. Mater.* **2017**, *29*, 1607017.
[78] C. Shen, L. Wang, A. Zhou, H. Zhang, Z. Chen, Q. Hu, G. Qin, *J. Electrochem. Soc.* **2017**, *164*, A2654.
[79] Z. Pourali, M. R. Sovizi, M. R. Yaftian, *J. Alloys Compd.* **2018**, *738*, 130.
[80] G. Zou, Z. Zhang, J. Guo, B. Liu, Q. Zhang, C. Fernandez, Q. Peng, *ACS Appl. Mater. Interfaces* **2016**, *8*, 22280.
[81] C. Zhan, M. Naguib, M. Lukatskaya, P. R. C. Kent, Y. Gogotsi, D. Jiang, *J. Phys. Chem. Lett.* **2018**, *9*, 1223.
[82] Y.-T. Du, X. Kan, F. Yang, L.-Y. Gan, U. Schwingenschlögl, *ACS Appl. Mater. Interfaces* **2018**, *10*, 32867.
[83] Y. Aierken, C. Sevik, O. Gulseren, F. M. Peeters, D. Cakir, *J. Mater. Chem. A* **2017**, *6*, 2337.
[84] C. Shen, L. Wang, A. Zhou, B. Wang, X. Wang, W. Lian, Q. Hu, G. Qin, X. Liu, *Nanomaterials* **2018**, *8*, 80.
[85] Z. Ma, X. Zhou, W. Deng, D. Lei, Z. Liu, *ACS Appl. Mater. Interfaces* **2018**, *10*, 3634.
[86] S. K. Kandasamy, K. Kandasamy, *J. Inorg. Organomet. Polym. Mater.* **2018**, *28*, 559.

[87] X.-M. Liu, Z. D. Huang, S. W. Oh, B. Zhang, P.-C. Ma, M. M. F. Yuen, J.-K. Kim, *Compos. Sci. Technol.* **2012**, *72*, 121.
[88] M.-Q. Zhao, C. E. Ren, Z. Ling, M. R. Lukatskaya, C. Zhang, K. L. Van Aken, M. W. Barsoum, Y. Gogotsi, *Adv. Mater.* **2015**, *27*, 339.
[89] W. Zheng, P. Zhang, J. Chen, W. B. Tian, Y. M. Zhang, Z. M. Sun, *J. Mater. Chem. A* **2018**, *6*, 3543.
[90] O. Mashtalir, M. R. Lukatskaya, M. Q. Zhao, M. W. Barsoum, Y. Gogotsi, *Adv. Mater.* **2015**, *27*, 3501.
[91] Y. Liu, W. Wang, Y. Ying, Y. Wang, X. Peng, *Dalton Trans.* **2015**, *44*, 7123.
[92] C. E. Ren, M.-Q. Zhao, T. Makaryan, J. Halim, M. Boota, S. Kota, B. Anasori, M. W. Barsoum, Y. Gogotsi, *ChemElectroChem* **2016**, *3*, 689.
[93] Z. Lin, D. Sun, Q. Huang, J. Yang, M. W. Barsoum, X. Yan, *J. Mater. Chem. A* **2015**, *3*, 14096.
[94] A. M. Chockla, K. C. Klavetter, C. B. Mullins, B. A. Korgel, *ACS Appl. Mater. Interfaces* **2012**, *4*, 4658.
[95] J. L. Tirado, *Mater. Sci. Eng. R* **2003**, *40*, 103.
[96] X.-L. Wu, Y.-G. Guo, L.-J. Wan, *Chem.: Asian J.* **2013**, *8*, 1948.
[97] A. A. Yaroshevsky, *Geochem. Int.* **2006**, *44*, 48.
[98] X. Zhou, Y. Liu, C. Du, Y. Ren, T. Mu, P. Zuo, G. Yin, Y. Ma, X. Cheng, Y. Gao, *J. Power Sources* **2018**, *381*, 156.
[99] X. Tang, G. Wen, Y. Song, *Appl. Surf. Sci.* **2018**, *436*, 398.
[100] G. A. Tritsaris, K. Zhao, O. U. Okeke, E. Kaxiras, *J. Phys. Chem. C* **2012**, *116*, 22212.
[101] S. R. Gowda, V. Pushparaj, S. Herle, G. Girishkumar, J. G. Gordon, H. Gullapalli, X. Zhan, P. M. Ajayan, A. L. M. Reddy, *Nano Lett.* **2012**, *12*, 6060.
[102] F. Kong, X. He, Q. Liu, X. Qi, D. Sun, Y. Zheng, R. Wang, Y. Bai, *Electrochem. Commun.* **2018**, *97*, 16.
[103] P. Zhang, Q. Zhu, Z. Guan, Q. Zhao, N. Sun, B. Xu, *ChemSusChem* **2019**, DOI 10.1002/cssc.201901497.
[104] H. Li, M. Lu, W. Han, H. Li, Y. Wu, W. Zhang, J. Wang, B. Zhang, *J. Energy Chem.* **2019**, *38*, 50.
[105] Y. Tian, Y. An, J. Feng, *ACS Appl. Mater. Interfaces* **2019**, *11*, 10004.
[106] C. Zhang, S.-H. Park, A. Seral-Ascaso, S. Barwich, N. McEvoy, C. S. Boland, J. N. Coleman, Y. Gogotsi, V. Nicolosi, *Nat. Commun.* **2019**, *10*, 849.
[107] Y. Zhang, Z. Mu, J. Lai, Y. Chao, Y. Yang, P. Zhou, Y. Li, W. Yang, Z. Xia, S. Guo, *ACS Nano* **2019**, *13*, 2167.
[108] J. Wozniak, M. Petrus, T. Cygan, A. Jastrzębska, T. Wojciechowski, W. Ziemkowska, A. Olszyna, *Ceram. Int.* **2019**, *45*, 6624.
[109] J. Halim, S. Kota, M. R. Lukatskaya, M. Naguib, M. Q. Zhao, E. J. Moon, J. Pitock, J. Nanda, S. J. May, Y. Gogotsi, M. W. Barsoum, *Adv. Funct. Mater.* **2016**, *26*, 3118.
[110] European Comission, *Report on Critical Raw Materials for the EU*, **2014**.
[111] M. R. Lukatskaya, O. Mashtalir, C. E. Ren, Y. Dall'Agnese, P. Rozier, P. L. Taberna, M. Naguib, P. Simon, M. W. Barsoum, Y. Gogotsi, *Science* **2013**, *341*, 1502.
[112] D. A. Stevens, J. R. Dahn, *J. Electrochem. Soc.* **2001**, *148*, A803.
[113] F. Li, C. R. Cabrera, J. Wang, Z. Chen, *RSC Adv.* **2016**, *6*, 81591.
[114] D. a. Webb, *J. Exp. Biol.* **1939**, *16*, 178.
[115] J. Song, Z. Yu, M. L. Gordin, S. Hu, R. Yi, D. Tang, T. Walter, M. Regula, D. Choi, X. Li, A. Manivannan, D. Wang, *Nano Lett.* **2014**, *14*, 6329.
[116] Y. Wang, C. Wang, Y. Wang, H. Liu, Z. Huang, *ACS Appl. Mater. Interfaces* **2016**, *8*, 18860.
[117] X. Wang, X. Shen, Y. Gao, Z. Wang, R. Yu, L. Chen, *J. Am. Chem. Soc.* **2015**, *137*, 2715.
[118] S. M. Bak, R. Qiao, W. Yang, S. Lee, X. Yu, B. Anasori, H. Lee, Y. Gogotsi, X. Q. Yang, *Adv. Energy Mater.* **2017**, *7*, 1700959.
[119] X. Lv, W. Wei, Q. Sun, L. Yu, B. Huang, Y. Dai, *ChemPhysChem* **2017**, *18*, 1627.
[120] Y. X. Yu, *J. Phys. Chem. C* **2016**, *120*, 5288.
[121] C. Shi, M. Beidaghi, M. Naguib, O. Mashtalir, Y. Gogotsi, S. J. L. Billinge, *Phys. Rev. Lett.* **2013**, *112*, 125501.
[122] J. Hassoun, F. Bonaccorso, M. Agostini, M. Angelucci, M. G. Betti, R. Cingolani, M. Gemmi, C. Mariani, S. Panero, V. Pellegrini, B. Scrosati, *Nano Lett.* **2014**, *14*, 4901.
[123] J. Hou, K. Tu, Z. Chen, *J. Phys. Chem. C* **2016**, *120*, 18473.
[124] M. Naguib, R. A. Adams, Y. Zhao, D. Zemlyanov, A. Varma, J. Nanda, V. G. Pol, *Chem. Commun.* **2017**, *53*, 6883.
[125] Q. Meng, J. Ma, Y. Zhang, Z. Li, C. Zhi, A. Hu, J. Fan, *Nanoscale* **2018**, *10*, 3385.
[126] J. Li, D. Yan, S. Hou, Y. Li, T. Lu, Y. Yao, L. Pan, *J. Mater. Chem. A* **2018**, *6*, 1234.
[127] X. Guo, X. Xie, S. Choi, Y. Zhao, H. Liu, C. Wang, S. Chang, G. Wang, *J. Mater. Chem. A* **2017**, *5*, 12445.
[128] Y. Xue, Q. Zhang, W. Wang, H. Cao, Q. Yang, L. Fu, *Adv. Energy Mater.* **2017**, *7*, 1602684.
[129] G. Lv, J. Wang, Z. Shi, L. Fan, *Mater. Lett.* **2018**, *219*, 45.
[130] Y. Wu, P. Nie, J. Wang, H. Dou, X. Zhang, *ACS Appl. Mater. Interfaces* **2017**, *9*, 39610.
[131] D. Zhao, M. Clites, G. Ying, S. Kota, J. Wang, V. Natu, X. Wang, M. Cao, E. Pomerantseva, M. W. Barsoum, *Chem. Commun.* **2018**, *54*, 2.
[132] V. Natu, M. Clites, E. Pomerantseva, M. W. Barsoum, *Mater. Res. Lett.* **2018**, *6*, 230.
[133] Y. Dong, Z.-S. Wu, S. Zheng, X. Wang, J. Qin, S. Wang, X. Shi, X. Bao, *ACS Nano* **2017**, *11*, 4792.
[134] Q. Meng, J. Ma, Y. Zhang, Z. Li, A. Hu, J.-J. Kai, J. Fan, *J. Mater. Chem. A* **2018**, *6*, 13652.
[135] I. Demiroglu, F. M. Peeters, O. Gülseren, D. Çaklr, C. Sevik, *J. Phys. Chem. Lett.* **2019**, *10*, 727.
[136] Y. Zhang, B. Guo, L. Hu, Q. Xu, Y. Li, D. Liu, M. Xu, *J. Alloys Compd.* **2018**, *732*, 448.
[137] X. Guo, J. Zhang, J. Song, W. Wu, H. Liu, G. Wang, *Energy Storage Mater.* **2018**, *14*, 306.
[138] M. Tao, Y. Zhang, R. Zhan, B. Guo, Q. Xu, M. Xu, *Mater. Lett.* **2018**, *230*, 173.
[139] W. Zhang, Z.-Z. Pan, W. Lv, R. Lv, W. Shen, F. Kang, Q.-H. Yang, Y. Weng, Z.-H. Huang, *Carbon N. Y.* **2019**, *153*, 625.
[140] X. Yu, J. Cheng, Z. Liu, Q. Li, W. Li, X. Yang, B. Xiao, *Chem. Phys. Lett.* **2015**, *629*, 36.
[141] J. Muldoon, C. B. Bucur, A. G. Oliver, T. Sugimoto, M. Matsui, H. S. Kim, G. D. Allred, J. Zajicek, Y. Kotani, *Energy Environ. Sci.* **2012**, *5*, 5941.
[142] H. D. Yoo, I. Shterenberg, Y. Gofer, G. Gershinsky, N. Pour, D. Aurbach, *Energy Environ. Sci.* **2013**, *6*, 2265.
[143] E. Levi, Y. Gofer, D. Aurbach, *Chem. Mater.* **2010**, *22*, 860.
[144] P. Jolibois, *C. R. Hebd. Seances Acad. Sci.* **1912**, *155*, 353.
[145] L. W. Gaddum, H. E. French, *J. Am. Chem. Soc.* **1927**, *49*, 1295.
[146] P. Novák, R. Imhof, O. Haas, *Electrochim. Acta* **1999**, *45*, 351.
[147] S. He, K. V. Nielson, J. Luo, T. L. Liu, *Energy Storage Mater.* **2017**, *8*, 184.
[148] C. B. Bucur, T. Gregory, A. G. Oliver, J. Muldoon, *J. Phys. Chem. Lett.* **2015**, *6*, 3578.
[149] M. Xu, S. Lei, J. Qi, Q. Dou, L. Liu, Y. Lu, Q. Huang, S. Shi, X. Yan, *ACS Nano* **2018**, *12*, 3733.
[150] M. Xu, N. Bai, H.-X. Li, C. Hu, J. Qi, X.-B. Yan, *Chin. Chem. Lett.* **2018**, *29*, 1313.
[151] Q. Gao, J. Come, M. Naguib, S. Jesse, Y. Gogotsi, N. Balke, *Faraday Discuss.* **2017**, *199*, 393.
[152] A. Byeon, M.-Q. Zhao, C. E. Ren, J. Halim, S. Kota, P. Urbankowski, B. Anasori, M. W. Barsoum, Y. Gogotsi, *ACS Appl. Mater. Interfaces* **2017**, *9*, 4296.
[153] M. Wang, C. Jiang, S. Zhang, X. Song, Y. Tang, H.-M. Cheng, *Nat. Chem.* **2018**, *10*, 667.
[154] A. L. Lipson, B. Pan, S. H. Lapidus, C. Liao, J. T. Vaughey, B. J. Ingram, *Chem. Mater.* **2015**, *27*, 8442.
[155] D. Aurbach, R. Skaletsky, Y. Gofer, *J. Electrochem. Soc.* **1991**, *138*, 3536.
[156] Z. Lu, A. Schechter, M. Moshkovich, D. Aurbach, *J. Electroanal. Chem.* **1999**, *466*, 203.
[157] A. Ponrouch, C. Frontera, F. Bardé, M. R. Palacín, *Nat. Mater.* **2016**, *15*, 169.
[158] F. Ambroz, T. J. Macdonald, T. Nann, *Adv. Energy Mater.* **2017**, *7*, 1602093.
[159] A. Vahidmohammadi, A. Hadjikhani, S. Shahbazmohamadi, M. Beidaghi, *ACS Nano* **2017**, *11*, 11135.
[160] Y. Xia, T. S. Mathis, M. Q. Zhao, B. Anasori, A. Dang, Z. Zhou, H. Cho, Y. Gogotsi, S. Yang, *Nature* **2018**, *557*, 409.
[161] B. Zhang, J. Zhu, P. Shi, W. Wu, F. Wang, *Ceram. Int.* **2019**, *45*, 8395.
[162] V. Palomares, P. Serras, I. Villaluenga, K. B. Hueso, J. Carretero-González, T. Rojo, *Energy Environ. Sci.* **2012**, *5*, 5884.
[163] B. Kishore, G. Venkatesh, N. Munichandraiah, *J. Electrochem. Soc.* **2016**, *163*, A2551.
[164] J. Han, M. Xu, Y. Niu, G.-N. Li, M. Wang, Y. Zhang, M. Jia, C. Ming Li, *Chem. Commun.* **2016**, *52*, 11274.
[165] H. Zhang, M. Hu, Q. Lv, Z. Huang, F. Kang, R. Lv, *Small* **2019**, 1902843.
[166] J. Ding, W. Hu, E. Paek, D. Mitlin, *Chem. Rev.* **2018**, *118*, 6457.
[167] X. Wang, S. Kajiyama, H. Iinuma, E. Hosono, S. Oro, I. Moriguchi, M. Okubo, A. Yamada, *Nat. Commun.* **2015**, *6*, 6544.
[168] J. Come, M. Naguib, P. Rozier, M. W. Barsoum, Y. Gogotsi, P.-L. Taberna, M. Morcrette, P. Simon, *J. Electrochem. Soc.* **2012**, *159*, A1368.

[169] Z. Li, G. Chen, J. Deng, D. Li, T. Yan, Z. An, L. Shi, D. Zhang, *ACS Sustainable Chem. Eng.* **2019**, *7*, 15394.
[170] J. Li, Q.-Q. Yang, Y.-X. Hu, M.-C. Liu, C. Lu, H. Zhang, L.-B. Kong, W.-W. Liu, W.-J. Niu, K. Zhao, Y.-C. Wang, F. Cheng, Z. M. Wang, Y.-L. Chueh, *ACS Sustainable Chem. Eng.* **2019**, *7*, 18375.
[171] X. Tang, H. Liu, X. Guo, S. Wang, W. Wu, A. K. Mondal, C. Wang, G. Wang, *Mater. Chem. Front.* **2018**, *2*, 1811.
[172] P. Yu, G. Cao, S. Yi, X. Zhang, C. Li, X. Sun, K. Wang, Y. Ma, *Nanoscale* **2018**, *10*, 5906.
[173] C. Wang, H. Xie, S. Chen, B. Ge, D. Liu, C. Wu, W. Xu, W. Chu, G. Babu, P. M. Ajayan, L. Song, *Adv. Mater.* **2018**, *30*, 1802525.
[174] W. Yang, J. Yang, J. J. Byun, F. P. Moissinac, J. Xu, S. J. Haigh, M. Domingos, M. A. Bissett, R. A. W. Dryfe, S. Barg, *Adv. Mater.* **2019**, *31*, 1902725.
[175] C. Zhang, L. McKeon, M. P. Kremer, S.-H. Park, O. Ronan, A. Seral-Ascaso, S. Barwich, C. Ó. Coileáin, N. McEvoy, H. C. Nerl, B. Anasori, J. N. Coleman, Y. Gogotsi, V. Nicolosi, *Nat. Commun.* **2019**, *10*, 1795.
[176] C. J. Zhang, M. P. Kremer, A. Seral-Ascaso, S.-H. Park, N. McEvoy, B. Anasori, Y. Gogotsi, V. Nicolosi, *Adv. Funct. Mater.* **2018**, *28*, 1705506.